

Angle-Domain Intelligent Reflecting Surface Systems: Design and Analysis

Xiaoling Hu, Caijun Zhong, and Zhaoyang Zhang

Abstract

This paper considers an angle-domain intelligent reflecting surface (IRS) system. We derive maximum likelihood (ML) estimators for the effective angles from the base station (BS) to the user and the effective angles of propagation from the IRS to the user. It is demonstrated that the accuracy of the estimated angles improves with the number of BS antennas. Also, deploying the IRS closer to the BS increases the accuracy of the estimated angle from the IRS to the user. Then, based on the estimated angles, we propose a joint optimization of BS beamforming and IRS beamforming, which achieves similar performance to two benchmark algorithms based on full CSI and the multiple signal classification (MUSIC) method respectively. Simulation results show that the optimized BS beam becomes more focused towards the IRS direction as the number of reflecting elements increases. Furthermore, we derive a closed-form approximation, upper bound and lower bound for the achievable rate. The analytical findings indicate that the achievable rate can be improved by increasing the number of BS antennas or reflecting elements. Specifically, the BS-user link and the BS-IRS-user link can obtain power gains of order N and NM^2 , respectively, where N is the antenna number and M is the number of reflecting elements.

I. INTRODUCTION

Wireless networks are anticipated to connect over 28.5 billion devices by the year 2022 [1], giving rise to questions of coverage, quality of service, reliability and energy consumption. Recently, the intelligent reflecting surface (IRS) has been proposed as a promising technology to address these questions, due to its features of both low energy consumption [2–8] and low hardware complexity [9, 10].

Specifically, an IRS is a meta-surface equipped with a large number of nearly passive, low-cost, reflecting elements with programmable parameters [11, 12]. Assisted by a smart controller, each reflecting element independently reflects the incident signal with adjustable phase shifts. With the ability to smartly alter phase shifts, the IRS can generate directional beams which are dynamically adjusted according to the operating requirements and conditions, thereby realizing programmable propagation environments [13]. Given that there is no amplifier used, the IRS is more energy-efficient than an Amplify-and-Forward (AF) relay. Another benefit of the IRS is that it can potentially be easily deployed, for example on building facades, due to its small size that is the consequence of an absence of radio frequency (RF) circuitry [14].

Hence, IRS-aided communications have attracted considerable attention as a promising means to realize dynamically adjustable wireless propagation channels, which can be used e.g. to fill coverage holes at a low cost. In particular, there have been a plethora of works on IRS beamforming, see e.g. [14–25]. In [15] and [16], the authors first presented the joint optimization of IRS beamforming and BS transmit beamforming. By applying a semidefinite relaxation (SDR) method, the total transmit power at the base station (BS) is minimized. Later on, [17] considered the minimization of the symbol error rate by iteratively optimizing the phase shifts and BS precoder, while [18] focused on maximizing the weighted sum-rate by adopting a Lagrangian dual transform technique under the assumption of discrete phase shifts. Finally, in [14], the energy efficiency maximization problem was solved via gradient descent search and sequential fractional programming. Besides, the integration of IRS with other promising technologies has also been investigated, for instance, non-orthogonal multiple access (NOMA) [19], millimeter wave (mmWave) [20], simultaneous wireless information and power transfer (SWIPT) [21], cognitive radio [26], two-way relaying [27], and physical layer security [28].

All the prior works on IRS beamforming assumed that perfect channel state information (CSI)

is available at both the BS and the IRS. How to obtain this CSI, however, is still a challenging issue for an IRS system due to the typically large number of reflecting elements and the passive architecture of the IRS. The typical channel estimation scheme is to estimate the cascaded IRS-aided channel by using various reflection patterns to train all the reflecting elements [29–32]. For example, an element-by-element ON/OFF-based reflection pattern was adopted in [29], while a new IRS reflection (phase-shift) pattern satisfying the unit-modulus constraint was proposed in [30]. However, the channel training overhead of such a scheme would become prohibitively high as the number of reflecting elements increases. Besides, since the CSI is estimated only at the transmitter and receiver, the IRS has no access to the CSI needed to perform beamforming. To tackle this problem, the works [16, 33] proposed a two-mode IRS model, where the IRS controller can switch between receiving mode for CSIs and reflecting mode for data transmission. However, the realization of a receiving mode would lead to higher hardware complexity as well as more power consumption, and diminishes the main strengths of the IRS, namely its low complexity and cost. To reduce the hardware cost, a semi-passive IRS architecture has been proposed [34, 35], where only a small proportion of IRS elements have the capability of both sensing and reflecting (referred to as semi-passive elements). As such, with the aid of these semi-passive elements, the IRS estimates the channels between itself and BS/users by leveraging on machine learning [34] or compressive sensing [35]. However, the computational complexity of the machine learning and compressive sensing methods is usually very high.

Motivated by these observations, in this paper, we propose an angle-domain IRS-aided system model, where effective angles are estimated by using a low-complexity method, and then exploited to design the BS beam and IRS phase shifts.¹ Although the angle-domain signal processing technique has been well studied in the existing works (e.g., [36–39]), this is the first time to introduce the concept of angle domain to deal with the channel estimation problem in the IRS-aided communication system. By exploiting angle sparsity, the training overhead as well as the computational complexity can be significantly reduced. The main advantages of this model are listed below:

- Only a very limited number of angles, instead of a large-scale channel matrix correspond-

¹Like the work [36], the proposed angle-domain framework exploits the angle sparsity. As such, the channel estimation and the corresponding beamforming design are more efficient compared to those of the conventional IRS-assisted communication. However, for non-sparse channels where there are a large number of scatters in the radio frequency environment, the proposed angle-domain design framework is no longer suitable, since the angular information detection may also be complicated and time-consuming.

ing to the IRS, are needed, thereby avoiding massive channel training overhead and high computational complexity.

- Due to the above, only a very small amount of CSI needs to be communicated from the BS to the IRS. This allows the passive IRS to obtain CSI without adding too much hardware complexity, by linking it to the BS via a low-capacity hardware line. As such, the BS and the IRS can exchange information (CSI and phase shifts), and thus the joint optimization of BS beamforming and IRS beamforming can be realized.

The contributions of this paper are summarized as follows:

- An angle-based channel estimation scheme with extremely low complexity has been proposed. In particular, the maximum likelihood (ML) estimators for effective angles from the BS to the user are presented, based on which the effective angles from the IRS to the user are derived.
- With a Gaussian model for the estimation error, we propose a joint optimization algorithm for BS beamforming and IRS beamforming, which achieves similar performance to two benchmark algorithms based on full CSI and the multiple signal classification (MUSIC) method respectively. Furthermore, we have proved mathematically that the average received signal power is non-decreasing after each iteration of the proposed algorithm.
- The expression for the achievable rate is presented, based on which a closed-form approximation, an upper bound for the achievable rate are derived. The analytical findings show that the BS-user link can obtain a power gain proportional to the number of antennas N , while the BS-IRS-user link can obtain a power gain of order NM^2 .

The remainder of the paper is organized as follows. In Section II, we introduce the angle-domain IRS-based system, while in Section III, we propose an angle estimation scheme. Based on the estimated effective angles, a joint optimization algorithm for BS beamforming and IRS beamforming is presented in Section IV. Then, we give a detailed analysis of the achievable rate in Section V. Numerical results and discussions are provided in Section VI, and finally Section VII concludes the paper.

Notation: Boldface lower case and upper case letters are used for column vectors and matrices, respectively. The superscripts $(\cdot)^*$, $(\cdot)^T$, $(\cdot)^H$, and $(\cdot)^{-1}$ stand for the conjugate, transpose, conjugate-transpose, and matrix inverse, respectively. Also, the Euclidean norm, absolute value,

Hadamard product are denoted by $\|\cdot\|$, $|\cdot|$ and \odot respectively. In addition, $\mathbb{E}\{\cdot\}$ is the expectation operator, and $\text{tr}(\cdot)$ represents the trace. $\text{Re}(\cdot)$ denotes the real part. For a matrix \mathbf{A} , $[\mathbf{A}]_{mn}$ denotes its entry in the m -th row and n -th column. For real numbers a and b , $\text{Remainder}(\frac{a}{b})$ and $\text{Quotient}(\frac{a}{b})$ respectively denote the Remainder and the quotient of a divided by b . Besides, j in $e^{j\theta}$ denotes the imaginary unit. Finally, $z \sim \mathcal{CN}(0, \sigma^2)$ denotes a circularly symmetric complex Gaussian random variable (RV) z with zero mean and variance σ^2 , and $z \sim \mathcal{N}(0, \sigma^2)$ denotes a real valued Gaussian RV.

II. SYSTEM MODEL

We consider an angle-domain IRS aided system, as illustrated in Fig.1, where the BS equipped with N antennas communicates with a single-antenna user assisted by an IRS with M reflecting elements. Both the BS and the IRS have uniform rectangular arrays (URA) with the sizes of $\sqrt{N}d_{\text{BS}} \times \sqrt{N}d_{\text{BS}}$ and $\sqrt{M}d_{\text{IRS}} \times \sqrt{M}d_{\text{IRS}}$ respectively, where d_{BS} is the distance between two adjacent BS antennas and d_{IRS} is the distance between two adjacent reflecting elements. Furthermore, the BS is connected with the IRS controller via a backhaul link so that they can exchange information (e.g. CSI and phase shifts).

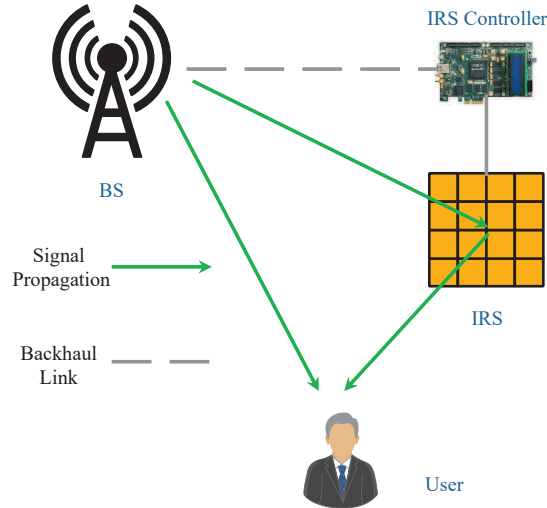


Fig. 1: Model of the angle-domain IRS aided system

An angle-domain Rician fading channel model is assumed, to model a channel with a line-of-sight (LOS) component. Such a channel corresponds to the practically desirable deployment of an IRS with LOS to both the BS and the user. Specifically, the channel from the BS to the IRS

can be expressed as

$$\mathbf{H}_{\text{B2I}} = \sqrt{\alpha_{\text{B2I}} \frac{v_{\text{B2I}}}{v_{\text{B2I}} + 1}} \mathbf{b} (\bar{\theta}_{\text{x-B2Ia}}, \bar{\theta}_{\text{y-B2Ia}}) \mathbf{a}^T (\bar{\theta}_{\text{x-B2I}}, \bar{\theta}_{\text{y-B2I}}) + \sqrt{\alpha_{\text{B2I}} \frac{1}{v_{\text{B2I}} + 1}} \tilde{\mathbf{H}}_{\text{B2I}}, \quad (1)$$

where $\tilde{\mathbf{H}}_{\text{B2I}}$ is the non-line of sight (NLOS) component, whose elements have the $\mathcal{CN}(0, 1)$ distribution, α_{B2I} models large-scale fading, v_{B2I} is the Rician K-factor, \mathbf{a} and \mathbf{b} are array steering vectors of the BS and the IRS, respectively. The two effective angles of departure (AODs), i.e., the phase differences between two adjacent antennas along the x and y axes, are respectively given by

$$\bar{\theta}_{\text{x-B2I}} = -\frac{2\pi d_{\text{BS}}}{\lambda} \cos \theta_{\text{B2I}} \cos \phi_{\text{B2I}}, \quad (2)$$

$$\bar{\theta}_{\text{y-B2I}} = -\frac{2\pi d_{\text{BS}}}{\lambda} \cos \theta_{\text{B2I}} \sin \phi_{\text{B2I}}, \quad (3)$$

where λ is the carrier wavelength, θ_{B2I} and ϕ_{B2I} are the elevation and azimuth AODs from the BS to the IRS, respectively. Similarly, the two effective angles of arrival (AOAs) are

$$\bar{\theta}_{\text{x-B2Ia}} = \frac{2\pi d_{\text{IRS}}}{\lambda} \cos \theta_{\text{B2Ia}} \cos \phi_{\text{B2Ia}}, \quad (4)$$

$$\bar{\theta}_{\text{y-B2Ia}} = \frac{2\pi d_{\text{IRS}}}{\lambda} \cos \theta_{\text{B2Ia}} \sin \phi_{\text{B2Ia}}, \quad (5)$$

where θ_{B2Ia} and ϕ_{B2Ia} are the elevation and azimuth AOAs at the IRS, respectively. Furthermore, we assume $d_{\text{BS}} = d_{\text{IRS}} = \frac{\lambda}{2}$.

Specifically, the n -th element of $\mathbf{a} (\bar{\theta}_{\text{x-B2I}}, \bar{\theta}_{\text{y-B2I}})$ and the m -th element of $\mathbf{b} (\bar{\theta}_{\text{x-B2I}}, \bar{\theta}_{\text{y-B2I}})$ are given by

$$a_n = e^{j(i_{N,n} \bar{\theta}_{\text{x-B2I}} + j_{N,n} \bar{\theta}_{\text{y-B2I}})}, \quad (6)$$

$$b_m = e^{j(i_{M,m} \bar{\theta}_{\text{x-B2I}} + j_{M,m} \bar{\theta}_{\text{y-B2I}})}, \quad (7)$$

where

$$i_{N,n} = \text{Remainder} \left(\frac{n-1}{\sqrt{N}} \right), n = 1, \dots, N, \quad (8)$$

$$j_{N,n} = \text{Quotient} \left(\frac{n-1}{\sqrt{N}} \right), n = 1, \dots, N, \quad (9)$$

$$i_{M,m} = \text{Remainder} \left(\frac{m-1}{\sqrt{M}} \right), m = 1, \dots, M, \quad (10)$$

$$j_{M,m} = \text{Quotient} \left(\frac{m-1}{\sqrt{M}} \right), m = 1, \dots, M. \quad (11)$$

Similarly, the channel from the IRS to the user is given by

$$\mathbf{h}_{\text{I2U}}^T = \sqrt{\alpha_{\text{I2U}} \frac{v_{\text{I2U}}}{v_{\text{I2U}} + 1}} \mathbf{b}^T (\bar{\theta}_{\text{x-I2U}}, \bar{\theta}_{\text{y-I2U}}) + \sqrt{\alpha_{\text{I2U}} \frac{1}{v_{\text{I2U}} + 1}} \tilde{\mathbf{h}}_{\text{I2U}}^T. \quad (12)$$

Also, the channel from the BS to the user can be expressed as

$$\mathbf{h}_{\text{B2U}}^T = \sqrt{\alpha_{\text{B2U}} \frac{v_{\text{B2U}}}{v_{\text{B2U}} + 1}} \mathbf{a}^T (\bar{\theta}_{\text{x-B2U}}, \bar{\theta}_{\text{y-B2U}}) + \sqrt{\alpha_{\text{B2U}} \frac{1}{v_{\text{B2U}} + 1}} \tilde{\mathbf{h}}_{\text{B2U}}^T. \quad (13)$$

During the data transmission, the BS transmits the signal $\mathbf{w}s$, where \mathbf{w} is the transmitting beam and s is the data intended for the user. Then, the signal received by the user is given by

$$y_{\text{U}} = (\mathbf{h}_{\text{B2U}}^T + \mathbf{h}_{\text{I2U}}^T \mathbf{\Theta} \mathbf{H}_{\text{B2I}}) \mathbf{w}s + n_{\text{U}}, \quad (14)$$

where \mathbf{w} is the BS transmitting beam, $n_{\text{U}} \sim \mathcal{CN}(0, \sigma_0^2)$ is the noise at the user, and the phase shift matrix $\mathbf{\Theta}$ is given by $\mathbf{\Theta} = \text{diag}(\boldsymbol{\xi})$ with the phase shift beam $\boldsymbol{\xi} = [e^{j\vartheta_1}, \dots, e^{j\vartheta_n}, \dots, e^{j\vartheta_M}]^T$.

To facilitate the design of BS transmitting beam \mathbf{w} and IRS phase shift beam $\boldsymbol{\xi}$, we first perform angle estimation as illustrated in the next section.

III. ANGULAR INFORMATION DETECTION METHOD

In this section, we propose a detection method to estimate the effective angles from the BS to the user ($\bar{\theta}_{\text{x-B2U}}$ and $\bar{\theta}_{\text{y-B2U}}$), based on which the effective angles from the IRS to the user ($\bar{\theta}_{\text{x-I2U}}$ and $\bar{\theta}_{\text{y-I2U}}$) are derived. Later, these effective angles will be exploited to design the BS beam and IRS phase shifts in Section IV.

During the angle estimation period, the IRS is turned off. The user transmits an unmodulated carrier at the power P_q to the BS. The received baseband signal at the BS is given by

$$\mathbf{r} = \mathbf{h}_{\text{B2U}}^* q + \mathbf{n}_{\text{BS}} = \sqrt{\frac{\alpha_{\text{B2U}} v_{\text{B2U}}}{v_{\text{B2U}} + 1}} \mathbf{a} (-\bar{\theta}_{\text{x-B2U}}, -\bar{\theta}_{\text{y-B2U}}) q + \sqrt{\frac{\alpha_{\text{B2U}}}{v_{\text{B2U}} + 1}} \tilde{\mathbf{h}}_{\text{B2U}}^* q + \mathbf{n}_{\text{BS}}, \quad (15)$$

where $q = \sqrt{P_q} e^{j\theta_q}$ is the baseband-equivalent representation of the unmodulated carrier, and $\mathbf{n}_{\text{BS}} \sim \mathcal{CN}(0, \sigma_{\text{BS},0}^2)$ is the noise at the BS.

In particular, the signal received by the n -th antenna is

$$\begin{aligned} r_n &= \sqrt{\frac{\alpha_{\text{B2U}} v_{\text{B2U}}}{v_{\text{B2U}} + 1}} a_n q + \sqrt{\frac{\alpha_{\text{B2U}}}{v_{\text{B2U}} + 1}} \tilde{h}_{\text{B2U},n} q + n_{\text{BS},n} \\ &= \sqrt{\frac{\alpha_{\text{U}} v_{\text{B2U}}}{v_{\text{B2U}} + 1}} e^{(-i_{N,n} \bar{\theta}_{\text{x-B2U}} - j_{N,n} \bar{\theta}_{\text{y-B2U}})} q + \sqrt{\frac{\alpha_{\text{B2U}}}{v_{\text{B2U}} + 1}} \tilde{h}_{\text{B2U},n} q + n_{\text{BS},n}. \end{aligned} \quad (16)$$

The phase of r_n can be decomposed as

$$\vartheta_n = \theta_q - i_{N,n} \bar{\theta}_{\text{x-B2U}} - j_{N,n} \bar{\theta}_{\text{y-B2U}} + e_n, \quad (17)$$

where e_n is the phase uncertainty caused by noise and NLOS paths.

Proposition 1: With a large Rician K-factor and a high received signal-to-noise ratio (SNR) at the BS, the phase uncertainty e_n is approximately circularly symmetric Gaussian $\mathcal{CN}(0, \sigma_e^2)$ with

$$\sigma_e^2 = \frac{4 - \pi}{8 v_{\text{B2U}}} + \frac{(4 - \pi)(v_{\text{B2U}} + 1)}{8 \alpha_{\text{B2U}} P_q v_{\text{B2U}}} \sigma_{\text{BS},0}^2. \quad (18)$$

Proof: See Appendix I. ■

Remark 1: From Proposition 1, we can observe that the phase uncertainty is a decreasing function with respect to the transmit power. Also, a larger Rician K-factor would lead to less phase uncertainty.

The observed phase difference between r_n and r_m is

$$\Delta \bar{\theta}_{n,m} = r_n - r_m = -(i_{N,n} - i_{N,m}) \bar{\theta}_{\text{x-B2U}} - (j_{N,n} - j_{N,m}) \bar{\theta}_{\text{y-B2U}} + \Delta e_{n,m}, \quad (19)$$

where $\Delta e_{n,m} = e_n - e_m \sim \mathcal{CN}(0, \sigma_{\text{pd}}^2)$ with $\sigma_{\text{pd}}^2 = 2\sigma_e^2$.

Then, we use the observed phase difference $\Delta \bar{\theta}_{n,m}$ to estimate $\bar{\theta}_{\text{x-B2U}}$ and $\bar{\theta}_{\text{y-B2U}}$. Specifically, we choose $\frac{N}{2}$ phase differences $\Delta \bar{\theta}_{n,m_n}, n = 1, \dots, \frac{N}{2}, m_n = N - n + 1$.

Theorem 1: The ML estimators for $\bar{\theta}_{\text{x-B2U}}$ and $\bar{\theta}_{\text{y-B2U}}$ are given by

$$\hat{\bar{\theta}}_{\text{x-B2U}} = -\frac{6 \sum_{n=1}^{N/2} (i_{N,n} - i_{N,m_n}) \Delta \bar{\theta}_{n,m_n}}{N(N-1)}, \quad (20)$$

$$\hat{\bar{\theta}}_{\text{y-B2U}} = -\frac{6 \sum_{n=1}^{N/2} (j_{N,n} - j_{N,m_n}) \Delta \bar{\theta}_{n,m_n}}{N(N-1)}. \quad (21)$$

Proof: See Appendix II. ■

Corollary 1: The effective angles $\bar{\theta}_{\text{x-B2U}}$ and $\bar{\theta}_{\text{y-B2U}}$ can be decomposed as

$$\bar{\theta}_{\text{x-B2U}} = \hat{\theta}_{\text{x-B2U}} + \epsilon_{\text{x-B2U}}, \quad (22)$$

$$\bar{\theta}_{\text{y-B2U}} = \hat{\theta}_{\text{y-B2U}} + \epsilon_{\text{y-B2U}}, \quad (23)$$

where $\epsilon_{\text{x-B2U}}$ and $\epsilon_{\text{y-B2U}}$ are estimation errors, which follow Guassian distribution $\mathcal{N}(0, \sigma_{\text{est}}^2)$ with the variance

$$\sigma_{\text{est}}^2 = \frac{6\sigma_{\text{pd}}^2}{N(N-1)}. \quad (24)$$

Proof: Starting from Theorem 1, and noticing that

$$\Delta\bar{\theta}_{n,m_n} \sim \mathcal{CN}\left(-(i_{N,n} - i_{N,m_n})\bar{\theta}_{\text{x-B2U}} - (j_{N,n} - j_{N,m_n})\bar{\theta}_{\text{y-B2U}}, \sigma_{\text{pd}}^2\right), \quad (25)$$

we can obtain the desired result. ■

Remark 2: Corollary 2 shows that the variance of the estimation error drops approximately inversely with the square of the antenna number, which indicates the great benefit of applying a large number of BS antennas in angle estimation.

With a LOS path between the BS and the user, their distance d_{B2U} can be obtained with high accuracy, by measuring time difference of arrival, i.e., wave propagation time from the user to the BS [40].

After obtaining the effective angles and the distance, we can estimate the location of the user as $(\hat{x}_{\text{U}}, \hat{y}_{\text{U}}, \hat{z}_{\text{U}})$ with

$$\hat{x}_{\text{U}} = -\frac{d_{\text{B2U}}\hat{\theta}_{\text{x-B2U}}}{\pi}, \quad (26)$$

$$\hat{y}_{\text{U}} = -\frac{d_{\text{B2U}}\hat{\theta}_{\text{y-B2U}}}{\pi}, \quad (27)$$

$$\hat{z}_{\text{U}} = -\frac{d_{\text{B2U}}\sqrt{\pi^2 - \hat{\theta}_{\text{x-B2U}}^2 - \hat{\theta}_{\text{y-B2U}}^2}}{\pi}, \quad (28)$$

where we assume the BS is located at $(0, 0, 0)$.

With the estimated user location $(\hat{x}_{\text{U}}, \hat{y}_{\text{U}}, \hat{z}_{\text{U}})$ and the perfectly known IRS location $(x_{\text{I}}, y_{\text{I}}, z_{\text{I}})$, the BS can calculate the effective angles from the IRS to the user as follows:

Lemma 1: The effective angles from the IRS to the user are

$$\hat{\theta}_{x-I2U} = \frac{(x_I - \hat{x}_U) \pi}{\hat{d}_{I2U}}, \quad (29)$$

$$\hat{\theta}_{y-I2U} = \frac{(y_I - \hat{y}_U) \pi}{\hat{d}_{I2U}}, \quad (30)$$

where

$$\hat{d}_{I2U} = \sqrt{(\hat{x}_U - x_I)^2 + (\hat{y}_U - y_I)^2 + (\hat{z}_U - z_I)^2}. \quad (31)$$

Proof: Lemma 1 is provable using elementary geometry. ■

Theorem 2: The effective angles from the IRS to the user can be decomposed into

$$\bar{\theta}_{x-I2U} = \hat{\theta}_{x-I2U} + \varphi_1 \epsilon_{x-B2U} + \varphi_2 \epsilon_{y-B2U}, \quad (32)$$

$$\bar{\theta}_{y-I2U} = \hat{\theta}_{y-I2U} + \varphi_2 \epsilon_{x-B2U} + \varphi_3 \epsilon_{y-B2U}, \quad (33)$$

with

$$\varphi_1 = Ra \left\{ 1 - \frac{\hat{\theta}_{x-I2U}^2}{\pi^2} + \frac{\hat{\theta}_{x-I2U}^2 \hat{\theta}_{z-I2U}}{\pi^3} \right\}, \quad (34)$$

$$\varphi_2 = Ra \left\{ -\frac{\hat{\theta}_{x-I2U} \hat{\theta}_{y-I2U}}{\pi^2} + \frac{\hat{\theta}_{x-I2U} \hat{\theta}_{y-I2U} \hat{\theta}_{z-I2U}}{\pi^3} \right\}, \quad (35)$$

$$\varphi_3 = Ra \left\{ 1 - \frac{\hat{\theta}_{y-I2U}^2}{\pi^2} + \frac{\hat{\theta}_{y-I2U}^2 \hat{\theta}_{z-I2U}}{\pi^3} \right\}, \quad (36)$$

where $Ra \triangleq \frac{d_{B2U}}{\hat{d}_{I2U}}$ and $\hat{\theta}_{z-I2U} \triangleq \frac{(z_I - \hat{z}_U) \pi}{\hat{d}_{I2U}}$.

Proof: See Appendix III. ■

Remark 3: Theorem 2 implies that in addition to the estimation error of $\hat{\theta}_{x-B2U}$ and $\hat{\theta}_{y-B2U}$, the accuracy of $\hat{\theta}_{x-I2U}$ and $\hat{\theta}_{y-I2U}$ is also significantly influenced by the distances of the IRS and the BS to the user. Specifically, the estimation error increases linearly with the ratio $Ra \triangleq \frac{d_{B2U}}{\hat{d}_{I2U}}$, implying that it is best to place the IRS close to the BS in terms of angle estimation accuracy.²

²It is worth noting that, assuming perfect CSI, it is desirable to place the IRS close to the BS or the user [10, 15]. However, in this paper, imperfect CSI is considered, as such placing the IRS close to the user would not necessarily improve the achievable due to the increased angle estimation error.

IV. JOINT OPTIMIZATION OF BS BEAMFORMING AND IRS BEAMFORMING

Using the estimated angles, in this section we aim to maximize the average received signal power:

$$P_r = \mathbb{E} \left\{ \left| (\mathbf{h}_{\text{B2U}}^T + \mathbf{h}_{\text{I2U}}^T \mathbf{\Theta} \mathbf{H}_{\text{B2I}}) \mathbf{w} \right|^2 \right\}, \quad (37)$$

by jointly optimizing BS beamforming and IRS beamforming.

We first give the expression of the average received signal power.

Proposition 2: The average received signal power is given by

$$P_r = \mathbf{w}^H \mathbf{T} \mathbf{w}, \quad (38)$$

with

$$\begin{aligned} \mathbf{T} \triangleq & \beta_{\text{B2I2U}} (\mathbf{\Theta} \bar{\mathbf{H}}_{\text{B2I}})^H \mathbf{B} \mathbf{\Theta} \bar{\mathbf{H}}_{\text{B2I}} + \sqrt{\beta_{\text{B2I2U}} \beta_{\text{B2U}}} \left((\mathbf{\Theta} \bar{\mathbf{H}}_{\text{B2I}})^H \mathbf{C} + \mathbf{C}^H \mathbf{\Theta} \bar{\mathbf{H}}_{\text{B2I}} \right) \\ & + \beta_{\text{B2U}} \mathbf{A} + \sigma_{\text{NLOS}}^2 \mathbf{I}_N, \end{aligned} \quad (39)$$

where

$$\bar{\mathbf{H}}_{\text{B2I}} \triangleq \mathbf{b} (\bar{\theta}_{\text{x-B2Ia}}, \bar{\theta}_{\text{y-B2Ia}}) \mathbf{a}^T (\bar{\theta}_{\text{x-B2I}}, \bar{\theta}_{\text{y-B2I}}) \quad (40)$$

$$\beta_{\text{B2I2U}} \triangleq \frac{\alpha_{\text{I2U}} \alpha_{\text{B2I}} v_{\text{B2I}} v_{\text{I2U}}}{(v_{\text{B2I}} + 1)(v_{\text{I2U}} + 1)}, \quad (41)$$

$$\beta_{\text{B2U}} \triangleq \frac{v_{\text{B2U}} \alpha_{\text{B2U}}}{v_{\text{B2U}} + 1}, \quad (42)$$

$$\sigma_{\text{NLOS}}^2 \triangleq M \frac{\alpha_{\text{I2U}} \alpha_{\text{B2I}}}{v_{\text{B2I}} + 1} \left(1 + \frac{v_{\text{B2I}}}{v_{\text{I2U}} + 1} \right) + \frac{\alpha_{\text{B2U}}}{v_{\text{B2U}} + 1}. \quad (43)$$

The elements of $\mathbf{A} \in \mathbb{C}^{N \times N}$, $\mathbf{B} \in \mathbb{C}^{M \times M}$ and $\mathbf{C} \in \mathbb{C}^{M \times N}$ are given by

$$[\mathbf{A}]_{mn} = [\hat{\mathbf{A}}]_{mn} \exp \left(-\frac{1}{2} \sigma_{\text{est}}^2 \{ i_{N,mn}^2 + j_{N,mn}^2 \} \right), \quad (44)$$

$$[\mathbf{B}]_{mn} = [\hat{\mathbf{B}}]_{mn} \exp \left(-\frac{1}{2} \sigma_{\text{est}}^2 \{ (i_{M,mn} \varphi_1 + j_{M,mn} \varphi_2)^2 + (j_{M,mn} \varphi_2 + i_{M,mn} \varphi_3)^2 \} \right), \quad (45)$$

$$[\mathbf{C}]_{mn} = [\hat{\mathbf{C}}]_{mn} \exp \left(-\frac{1}{2} \sigma_{\text{est}}^2 \{ (i_{M,m} \varphi_1 + j_{M,m} \varphi_2 - i_{N,n})^2 + (i_{M,m} \varphi_2 + j_{M,m} \varphi_3 - j_{N,n})^2 \} \right), \quad (46)$$

where $i_{M,mn} \triangleq (i_{M,n} - i_{M,m})$, $j_{M,mn} \triangleq (j_{M,n} - j_{M,m})$, $\hat{\mathbf{A}} \triangleq \mathbf{a}^* \left(\hat{\theta}_{\text{x-B2U}}, \hat{\theta}_{\text{y-B2U}} \right) \mathbf{a}^T \left(\hat{\theta}_{\text{x-B2U}}, \hat{\theta}_{\text{y-B2U}} \right)$, $\hat{\mathbf{B}} \triangleq \mathbf{b}^* \left(\hat{\theta}_{\text{x-I2U}}, \hat{\theta}_{\text{y-I2U}} \right) \mathbf{b}^T \left(\hat{\theta}_{\text{x-I2U}}, \hat{\theta}_{\text{y-I2U}} \right)$ and $\hat{\mathbf{C}} \triangleq \mathbf{b}^* \left(\hat{\theta}_{\text{x-I2U}}, \hat{\theta}_{\text{y-I2U}} \right) \mathbf{a}^T \left(\hat{\theta}_{\text{x-B2U}}, \hat{\theta}_{\text{y-B2U}} \right)$.

Proof: See Appendix IV. ■

Then the optimization problem can be formulated as:

$$\begin{aligned}
& \max_{\{\mathbf{\Theta}, \mathbf{w}\}} P_r = \mathbf{w}^H \mathbf{T} \mathbf{w}, \\
& \text{s. t.} \quad \|\mathbf{w}\|^2 \leq P_{BS}, \\
& \quad \quad \quad |[\mathbf{\Theta}]_{ii}| = 1, i = 1, \dots, M,
\end{aligned} \tag{47}$$

where P_{BS} is the maximum transmit power at the BS.

Since the phase shift matrix $\mathbf{\Theta}$ and the BS beam \mathbf{w} are coupled, the above optimization problem (47) is difficult to solve. Responding to this, we will first optimize \mathbf{w} by fixing $\mathbf{\Theta}$ and then update $\mathbf{\Theta}$ by fixing \mathbf{w} respectively. As such, we can obtain sub-optimal solutions for both \mathbf{w} and $\mathbf{\Theta}$ by performing this successive refinement process iteratively.

A. BS beamforming

By fixing the phase shift matrix $\mathbf{\Theta}$, we can simplify (47) to

$$\begin{aligned}
& \max_{\{\mathbf{w}\}} P(\mathbf{w}) = \mathbf{w}^H \mathbf{T} \mathbf{w}, \\
& \text{s. t.} \quad \|\mathbf{w}\|^2 \leq P_{BS}.
\end{aligned} \tag{48}$$

The above problem is a convex problem equivalent to

$$\begin{aligned}
& \min_{\{\mathbf{w}\}} L(\mathbf{w}, \mu) = -\mathbf{w}^H \mathbf{T} \mathbf{w} + \mu (|\mathbf{w}|^2 - P_{BS}), \\
& \text{s. t.} \quad \mu > 0,
\end{aligned} \tag{49}$$

where $\mu > 0$ is the Lagrangian multiplier.

The Karush-Kuhn-Tucker (KKT) conditions are

$$\nabla_{\mathbf{w}} L(\mathbf{w}, \mu) = -2\mathbf{T}\mathbf{w} + 2\mu\mathbf{w} = 0, \tag{50}$$

$$\nabla_{\mu} L(\mathbf{w}, \mu) = |\mathbf{w}|^2 - P_{BS} = 0, \tag{51}$$

based on which, we have

$$\mathbf{w} = \sqrt{P_{BS}} \mathbf{t}_{\max}, \tag{52}$$

where \mathbf{t}_{\max} is the eigenvector of \mathbf{T} corresponding to the largest eigenvalue.

B. IRS beamforming

For a given \mathbf{w} , the optimization problem (47) can be rewritten as

$$\begin{aligned}
\max_{\{\boldsymbol{\Theta}\}} P(\boldsymbol{\Theta}) &\triangleq \beta_{\text{B2I2U}} \mathbf{w}^H \sqrt{\beta_{\text{B2I2U}} \beta_{\text{B2U}}} (\boldsymbol{\Theta} \bar{\mathbf{H}}_{\text{B2I}})^H \mathbf{B} \boldsymbol{\Theta} \bar{\mathbf{H}}_{\text{B2I}} \mathbf{w} \\
&+ \sqrt{\beta_{\text{B2I2U}} \beta_{\text{B2U}}} \left(\mathbf{w}^H (\boldsymbol{\Theta} \bar{\mathbf{H}}_{\text{B2I}})^H \mathbf{C} \mathbf{w} + \mathbf{w}^H \mathbf{C}^H \boldsymbol{\Theta} \bar{\mathbf{H}}_{\text{B2I}} \mathbf{w} \right) \\
&+ \beta_{\text{B2U}} \mathbf{w}^H \mathbf{A} \mathbf{w} + \sigma_{\text{NLOS}}^2 \mathbf{w}^H \mathbf{w} \\
\text{s. t.} \quad &|[\boldsymbol{\Theta}]_{ii}| = 1, i = 1, \dots, M.
\end{aligned} \tag{53}$$

According to the rule that $\mathbf{E}^H \mathbf{X}^H \mathbf{F} = \mathbf{x}^H (\mathbf{E}^* \odot \mathbf{F})$ with $\mathbf{X} = \text{diag}(\mathbf{x})$, the objective function can be rewritten as

$$\begin{aligned}
P(\boldsymbol{\Theta}) &= \beta_{\text{B2I2U}} \text{tr} \left(\boldsymbol{\Theta}^H \mathbf{B} \boldsymbol{\Theta} \bar{\mathbf{H}}_{\text{B2I}} \mathbf{w} \mathbf{w}^H \bar{\mathbf{H}}_{\text{B2I}}^H \right) \\
&+ \sqrt{\beta_{\text{B2I2U}} \beta_{\text{B2U}}} \boldsymbol{\xi}^H (\bar{\mathbf{H}}_{\text{B2I}}^* \mathbf{w}^* \odot \mathbf{C} \mathbf{w}) + \sqrt{\beta_{\text{B2I2U}} \beta_{\text{B2U}}} (\bar{\mathbf{H}}_{\text{B2I}}^T \mathbf{w}^T \odot \mathbf{w}^H \mathbf{C}^H) \boldsymbol{\xi} \\
&+ \beta_{\text{B2U}} \mathbf{w}^H \mathbf{A} \mathbf{w} + \sigma_{\text{NLOS}}^2 \mathbf{w}^H \mathbf{w}.
\end{aligned} \tag{54}$$

Using the property that $\mathbf{X}^H \mathbf{E} \mathbf{Y} \mathbf{F} = \mathbf{x}^H (\mathbf{E} \odot \mathbf{F}^T) \mathbf{y}$ with $\mathbf{X} = \text{diag}(\mathbf{x})$ and $\mathbf{Y} = \text{diag}(\mathbf{y})$, the above equation can be further expressed as

$$\begin{aligned}
P(\boldsymbol{\xi}) &= \beta_{\text{B2I2U}} \boldsymbol{\xi}^H \left(\mathbf{B} \odot (\bar{\mathbf{H}}_{\text{B2I}} \mathbf{w} \mathbf{w}^H \bar{\mathbf{H}}_{\text{B2I}}^H)^T \right) \boldsymbol{\xi} \\
&+ \sqrt{\beta_{\text{B2I2U}} \beta_{\text{B2U}}} \boldsymbol{\xi}^H (\bar{\mathbf{H}}_{\text{B2I}}^* \mathbf{w}^* \odot \mathbf{C} \mathbf{w}) + \sqrt{\beta_{\text{B2I2U}} \beta_{\text{B2U}}} (\bar{\mathbf{H}}_{\text{B2I}}^T \mathbf{w}^T \odot \mathbf{w}^H \mathbf{C}^H) \boldsymbol{\xi} \\
&+ \beta_{\text{B2U}} \mathbf{w}^H \mathbf{A} \mathbf{w} + \sigma_{\text{NLOS}}^2 \mathbf{w}^H \mathbf{w},
\end{aligned} \tag{55}$$

based on which, the optimization problem can be reformulated as

$$\begin{aligned}
\max_{\{\boldsymbol{\xi}\}} P(\boldsymbol{\xi}) &= \beta_{\text{B2I2U}} \boldsymbol{\xi}^H \left(\mathbf{B} \odot (\bar{\mathbf{H}}_{\text{B2I}} \mathbf{w} \mathbf{w}^H \bar{\mathbf{H}}_{\text{B2I}}^H)^T \right) \boldsymbol{\xi} \\
&+ \sqrt{\beta_{\text{B2I2U}} \beta_{\text{B2U}}} \boldsymbol{\xi}^H (\bar{\mathbf{H}}_{\text{B2I}}^* \mathbf{w}^* \odot \mathbf{C} \mathbf{w}) + \sqrt{\beta_{\text{B2I2U}} \beta_{\text{B2U}}} (\bar{\mathbf{H}}_{\text{B2I}}^T \mathbf{w}^T \odot \mathbf{w}^H \mathbf{C}^H) \boldsymbol{\xi} \\
&+ \beta_{\text{B2U}} \mathbf{w}^H \mathbf{A} \mathbf{w} + \sigma_{\text{NLOS}}^2 \mathbf{w}^H \mathbf{w} \\
\text{s. t.} \quad &|\xi_i| = 1, i = 1, \dots, M.
\end{aligned} \tag{56}$$

Since $|\xi_i| = 1$, we have $\text{tr}(\boldsymbol{\xi} \boldsymbol{\xi}^H) = M$. In order to deal with the non-convex constraint of $|\xi_i| = 1$, we relax the problem (56) into the following optimization problem with a convex ℓ_∞

constraint:

$$\begin{aligned} \max_{\{\boldsymbol{\xi}\}} \quad & P(\boldsymbol{\xi}) \\ \text{s. t.} \quad & \text{tr}(\boldsymbol{\xi}\boldsymbol{\xi}^H) = M, \\ & \|\boldsymbol{\xi}\|_\infty \leq 1. \end{aligned} \quad (57)$$

Since the ℓ_∞ constraint is non-differentiable, we instead use the ℓ_p with a large p to approximate ℓ_∞ , $\lim_{p \rightarrow \infty} \ell_p = \ell_\infty$. To solve (57), we incorporate the second constraint by exploiting the barrier method with the logarithmic barrier function $F(x)$ to approximate the penalty of violating the ℓ_p constraint,

$$F(x) = \begin{cases} -\frac{1}{\kappa} \ln(x), & x > 0 \\ \infty, & x \leq 0 \end{cases},$$

where κ is used to scale the barrier function penalty. As such, the optimization problem can be rewritten as:

$$\begin{aligned} \min_{\{\boldsymbol{\xi}\}} G(\boldsymbol{\xi}) &= F\left(1 - \|\boldsymbol{\xi}\|_p\right) - \beta_{\text{B2I2U}} \boldsymbol{\xi}^H \left(\mathbf{B} \odot (\bar{\mathbf{H}}_{\text{B2I}} \mathbf{w} \mathbf{w}^H \bar{\mathbf{H}}_{\text{B2I}}^H)^T\right) \boldsymbol{\xi} \\ &\quad - \sqrt{\beta_{\text{B2I2U}} \beta_{\text{B2U}}} \boldsymbol{\xi}^H (\bar{\mathbf{H}}_{\text{B2I}}^* \mathbf{w}^* \odot \mathbf{C} \mathbf{w}) - \sqrt{\beta_{\text{B2I2U}} \beta_{\text{B2U}}} (\bar{\mathbf{H}}_{\text{B2I}}^T \mathbf{w}^T \odot \mathbf{w}^H \mathbf{C}^H) \boldsymbol{\xi} \\ \text{s. t.} \quad & \text{tr}(\boldsymbol{\xi}\boldsymbol{\xi}^H) = M. \end{aligned} \quad (58)$$

Due to the non-convex constraint $\text{tr}(\boldsymbol{\xi}\boldsymbol{\xi}^H) = M$, the optimization problem (58) is non-convex. Next, we try to solve the above optimization problem by exploiting a gradient method. As such, sub-optimal solutions can be obtained. The gradient of the objective function $G(\boldsymbol{\xi})$ can be calculated as

$$\nabla_{\boldsymbol{\xi}} G(\boldsymbol{\xi}) = \frac{\|\boldsymbol{\xi}\|_p^{1-p} \boldsymbol{\zeta}}{2\kappa (1 - \|\boldsymbol{\xi}\|_p)} - \nabla_{\boldsymbol{\xi}} P(\boldsymbol{\xi}), \quad (59)$$

where

$$\boldsymbol{\zeta} = [\xi_1 |\xi_1|^{p-2}, \xi_2 |\xi_2|^{p-2}, \dots, \xi_M |\xi_M|^{p-2}]^T. \quad (60)$$

And the gradient $\nabla_{\boldsymbol{\xi}} P(\boldsymbol{\xi})$ can be computed as

$$\nabla_{\boldsymbol{\xi}} P(\boldsymbol{\xi}) = 2\beta_{\text{B2I2U}} \left(\mathbf{B} \odot (\bar{\mathbf{H}}_{\text{B2I}} \mathbf{w} \mathbf{w}^H \bar{\mathbf{H}}_{\text{B2I}}^H)^T\right) \boldsymbol{\xi} + 2\sqrt{\beta_{\text{B2I2U}} \beta_{\text{B2U}}} \text{Re}((\bar{\mathbf{H}}_{\text{B2I}}^* \mathbf{w}^* \odot \mathbf{C} \mathbf{w}) \mathbf{1}_N), \quad (61)$$

where $\mathbf{1}_N$ is a $N \times 1$ vector whose elements all equal to 1.

Algorithm 1 IRS Beamforming Algorithm

- 1: **Initialization** : Given a feasible phase shift vector ξ_1 , a large $p > 0$, the iteration index $i = 0$, the maximum iterations $N_{\text{iter}} > 0$, halting criterion $\varepsilon > 0$ and the barrier coefficient $\kappa > 0$.
- 2: **repeat**
- 3: $i \leftarrow i + 1$.
- 4: Compute the gradient as per (62).
- 5: Compute the search direction \mathbf{g}_p as per (63).
- 6: For $0 \leq \varpi \leq 1$, searching for it by

$$\varpi^* = \arg \max_{\varpi} P \left((1 - \varpi) \xi_i + \varpi \sqrt{M} \frac{\mathbf{g}_p}{\|\mathbf{g}_p\|^2} \right). \quad (64)$$

- 7: Update:

$$\xi_{i+1} = (1 - \varpi^*) \xi_i + \varpi^* \sqrt{M} \frac{\mathbf{g}_p}{\|\mathbf{g}_p\|^2}. \quad (65)$$

- 8: **until** $|P(\xi_{i+1}) - P(\xi_i)| \leq \varepsilon$ or $i \geq N_{\text{iter}}$.
 - 9: **Output** : $\xi^* = \exp[j\text{angle}(\xi_i)]$.
-

Thus, $\nabla_{\xi} G(\xi)$ can be rewritten as

$$\begin{aligned} \nabla_{\xi} G(\xi) = & -2\beta_{\text{B2IU}} \left(\mathbf{B} \odot (\bar{\mathbf{H}}_{\text{B2I}} \mathbf{w} \mathbf{w}^H \bar{\mathbf{H}}_{\text{B2I}}^H)^T \right) \xi \\ & - 2\sqrt{\beta_{\text{B2IU}} \beta_{\text{B2U}}} \text{Re} \left((\bar{\mathbf{H}}_{\text{B2I}}^* \mathbf{w}^* \odot \mathbf{C} \mathbf{w}) \mathbf{1}_N \right) + \frac{\|\xi\|_p^{1-p} \zeta}{2\kappa \left(1 - \|\xi\|_p \right)}. \end{aligned} \quad (62)$$

Due to the constraint $\text{tr}(\xi \xi^H) = M$, we project $\mathbf{g}_{\text{gd}} = -\nabla_{\xi} G(\xi)$ into the tangent plane of $\text{tr}(\xi \xi^H) = M$:

$$\mathbf{g}_p = \mathbf{g}_{\text{gd}} - \frac{\mathbf{g}_{\text{gd}}^T \xi^* \xi}{\|\xi\|^2}. \quad (63)$$

Then we use \mathbf{g}_p as the search direction. Algorithm 1 provides the pseudo-code for the process. For convenience, we collect the principal and important parameters and variables in Table I.

Proposition 3: The constant-modulus constraint $|\xi_i| = 1, i = 1, \dots, M$ is satisfied.

Proof: See Appendix V. ■

C. Joint optimization of BS beamforming and IRS beamforming

According to IV-A and IV-B, a joint optimization scheme is developed in Algorithm 2, where the BS beam and phase shift beam are iteratively optimized.

Proposition 4: The joint optimization algorithm always guarantees $P(\mathbf{w}_{i+1}, \xi_{i+1}) \geq P(\mathbf{w}_i, \xi_i)$.

Parameter	Definition
Variable \mathbf{w}	Transmit beamforming vector.
Variable $\boldsymbol{\xi}$	Phase shift vector.
Variable $\boldsymbol{\Theta}$	Phase shift matrix $\boldsymbol{\Theta} = \text{diag}(\boldsymbol{\xi})$
$\beta_{\text{B2IU}}, \beta_{\text{B2U}}$	Defined by (41) and (42), respectively.
\mathbf{B}, \mathbf{C}	Defined by (45) and (46), respectively.
\mathbf{H}_{B2I}	Defined by (40).

TABLE I: Parameter Table.

Algorithm 2 Joint Optimization Algorithm

-
- 1: **Initialization** : Given feasible initial solutions $\boldsymbol{\xi}_0$, \mathbf{w}_0 and the iteration index $i = 0$.
 - 2: **repeat**
 - 3: Perform BS beamforming: According to $\boldsymbol{\xi}_0$, optimize the BS beam by invoking the result (52) in IV-A, which yields \mathbf{w}_{i+1} .
 - 4: Perform IRS beamforming: Based on \mathbf{w}_{i+1} , optimize the transmit beamformer via Algorithm 1, which yields $\boldsymbol{\xi}_{i+1}$.
 - 5: $i \leftarrow i + 1$.
 - 6: **until** $\boldsymbol{\xi}_i$ and \mathbf{w}_i are converged.
 - 7: **Output** : $\boldsymbol{\xi}^* = \boldsymbol{\xi}_i$ and $\mathbf{w}^* = \mathbf{w}_i$.
-

Proof: 1) Proof of $P(\mathbf{w}_{i+1}, \boldsymbol{\xi}_{i+1}) \geq P(\mathbf{w}_i, \boldsymbol{\xi}_{i+1})$

By fixing $\boldsymbol{\xi}$, the optimization of \mathbf{w} is a convex problem. And, \mathbf{w}_{i+1} is the optimal solution corresponding to the phase shift beam $\boldsymbol{\xi}_{i+1}$. Thus, we have

$$P(\mathbf{w}_{i+1}, \boldsymbol{\xi}_{i+1}) \geq P(\mathbf{w}_i, \boldsymbol{\xi}_{i+1}). \quad (66)$$

2) Proof of $P(\mathbf{w}_{i+1}, \boldsymbol{\xi}_{i+1}) \geq P(\mathbf{w}_{i+1}, \boldsymbol{\xi}_i)$

Fixing \mathbf{w}_{i+1} , the Taylor expansion of $P(\mathbf{w}_{i+1}, \boldsymbol{\xi}_{i+1})$ can be expressed as

$$\begin{aligned} P(\mathbf{w}_{i+1}, \boldsymbol{\xi}_{i+1}) &= P(\mathbf{w}_{i+1}, \boldsymbol{\xi}_i) + \left(\nabla_{\boldsymbol{\xi}_i} P \right)^H \{ P(\mathbf{w}_{i+1}, \boldsymbol{\xi}_{i+1}) - P(\mathbf{w}_{i+1}, \boldsymbol{\xi}_i) \} \\ &\quad + o \left\{ (P(\mathbf{w}_{i+1}, \boldsymbol{\xi}_{i+1}) - P(\mathbf{w}_{i+1}, \boldsymbol{\xi}_i))^2 \right\}. \end{aligned} \quad (67)$$

Based on (65) in Algorithm 1, for any $\varpi \rightarrow 0$, the above equation can be written as

$$\begin{aligned} P(\mathbf{w}_{i+1}, \boldsymbol{\xi}_{i+1}) &= P(\mathbf{w}_{i+1}, \boldsymbol{\xi}_i) + \left(\nabla_{\boldsymbol{\xi}_i} P \right)^H \sqrt{M} \frac{\mathbf{g}_p}{\|\mathbf{g}_p\|^2} \varpi^* + o \{ \varpi^{*2} \} \\ &\approx P(\mathbf{w}_{i+1}, \boldsymbol{\xi}_i) + \left(\nabla_{\boldsymbol{\xi}_i} P \right)^H \mathbf{g}_p \frac{\sqrt{M}}{\|\mathbf{g}_p\|^2} \varpi^*. \end{aligned} \quad (68)$$

Next, we focus on the calculation of $\left(\nabla_{\boldsymbol{\xi}_i} P\right)^H \mathbf{g}_p$.

$$\left(\nabla_{\boldsymbol{\xi}_i} P\right)^H \mathbf{g}_p = \left(\mathbf{g}_{\text{gd}} + \nabla_{\boldsymbol{\xi}_i} F(1 - \|\boldsymbol{\xi}_i\|^2)\right)^H \mathbf{g}_p. \quad (69)$$

Recall that $\nabla_{\boldsymbol{\xi}_i} F(1 - \|\boldsymbol{\xi}_i\|^2) = \frac{\|\boldsymbol{\xi}_i\|_p^{1-p} \boldsymbol{\Omega} \boldsymbol{\xi}_i}{2\kappa(1 - \|\boldsymbol{\xi}_i\|_p)}$ with $\boldsymbol{\Omega} = \text{diag}(|\xi_1|^{p-2}, |\xi_2|^{p-2}, \dots, |\xi_M|^{p-2})$, and $\mathbf{g}_p = \mathbf{g}_{\text{gd}} - \frac{\mathbf{g}_{\text{gd}}^T \boldsymbol{\xi}_i^* \boldsymbol{\xi}_i}{\|\boldsymbol{\xi}_i\|^2}$. We have $\left(\nabla_{\boldsymbol{\xi}_i} F(1 - \|\boldsymbol{\xi}_i\|^2)\right)^H \mathbf{g}_p = 0$, and thus the above equation can be calculated as

$$\left(\nabla_{\boldsymbol{\xi}_i} P\right)^H \mathbf{g}_p = \mathbf{g}_{\text{gd}}^H \mathbf{g}_p = \|\mathbf{g}_{\text{gd}}\|^2 (1 - (\cos \varrho)^2) \geq 0, \quad (70)$$

where $\varrho = \arccos\left(\frac{\mathbf{g}_{\text{gd}}^H \boldsymbol{\xi}_i}{\|\mathbf{g}_{\text{gd}}\| \|\boldsymbol{\xi}_i\|}\right)$ is the angle between vectors \mathbf{g}_{gd} and $\boldsymbol{\xi}_i$.

Substituting (70) into (68), we obtain

$$P(\mathbf{w}_{i+1}, \boldsymbol{\xi}_{i+1}) - P(\mathbf{w}_{i+1}, \boldsymbol{\xi}_i) = \left(\nabla_{\boldsymbol{\xi}_i} P\right)^H \mathbf{g}_p \frac{\sqrt{M}}{\|\mathbf{g}_p\|^2} \varpi^* \geq 0. \quad (71)$$

To this end, combining 1) and 2), we have

$$P(\mathbf{w}_{i+1}, \boldsymbol{\xi}_{i+1}) \geq P(\mathbf{w}_{i+1}, \boldsymbol{\xi}_i) \geq P(\mathbf{w}_i, \boldsymbol{\xi}_i). \quad (72)$$

■

Remark 4: Our method of iteratively optimizing the transmit beam and the phase shift beam can provide an efficient way to gradually increase the average received signal power, although only a sub-optimal solution can be ensured due to the non-convexity of the problem.

Remark 5: For the BS beamforming scheme, the complexity is consumed by the eigenvector calculation. Therefore, the complexity order of BS beamforming is $\mathcal{O}(N^3)$.

For the IRS beamforming algorithm, the computational complexity is mainly determined by the calculation of the gradient (62), involving computing the ℓ_p norm and the matrix multiplication $\left(\mathbf{B} \odot (\bar{\mathbf{H}}_{\text{B2I}} \mathbf{w} \mathbf{w}^H \bar{\mathbf{H}}_{\text{B2I}}^H)^T\right) \boldsymbol{\xi}$. Hence, the complexity order of Algorithm 1 for each iteration is $\mathcal{O}(M^2 + pM)$.

Finally, the overall complexity order of the joint optimization algorithm for each iteration is given by $\mathcal{O}(N_{\text{iter}}(M^2 + pM) + N^3)$, where N_{iter} is specified in Algorithm 1.

V. ACHIEVABLE RATE ANALYSIS

In this section, we will present detailed analysis of the achievable rate.

Theorem 3: The achievable rate is given by

$$R = \log_2 \left(1 + \frac{\tilde{\mathbf{w}}^H \mathbf{T} \tilde{\mathbf{w}}}{\sigma_0^2} \right), \quad (73)$$

where $\tilde{\mathbf{w}} \triangleq \sqrt{P_{\text{BS}}} \mathbf{t}_{\text{max}}$.

Proof: Starting from Proposition 2, the result is readily obtained. \blacksquare

Theorem 3 presents an expression for the achievable rate which quantifies the impact of key system parameters, such as the number of BS antennas and reflecting elements, as well as the impact of estimation error on the achievable rate. For instance, it can be seen that the SNR is related to \mathbf{T} . From the expression of \mathbf{T} which is defined in Proposition 2, we can conclude that the SNR drops nearly exponentially with the variance of the angle estimation error. This is because inaccurate estimated angles makes it difficult to generate highly directional beams, thereby causing severe power loss.

Corollary 2: Assuming a large Rician K -factor and that the IRS and the user are in the similar direction, the achievable rate can be approximated as

$$R_{\text{approx}} = \log_2 \left(1 + \frac{P_{\text{BS}} \Omega}{\sigma_0^2} \right), \quad (74)$$

where

$$\begin{aligned} \Omega \triangleq & N\beta_{\text{B2I2U}} \sum_{m=1}^M \sum_{n=1}^M \xi_m^* \xi_n [\mathbf{B}]_{mn} b_{\text{B2Ia},m}^* b_{\text{B2Ia},n} \\ & + 2\sqrt{\beta_{\text{B2I2U}}\beta_{\text{B2U}}} \text{Re} \left\{ \sum_{m=1}^M \xi_m^* b_{\text{B2Ia},m}^* \left(\sum_{i=1}^N [\mathbf{C}]_{mi} a_{\text{B2I},i}^* \right) \right\} + N\beta_{\text{B2U}} + N\sigma_{\text{NLOS}}^2, \end{aligned} \quad (75)$$

where $a_{\text{B2I},m}$ and $b_{\text{B2Ia},m}$ are the m -th elements of $\mathbf{a}^T (\bar{\theta}_{\text{x-B2I}}, \bar{\theta}_{\text{y-B2I}})$ and $\mathbf{b}^T (\bar{\theta}_{\text{x-B2Ia}}, \bar{\theta}_{\text{y-B2Ia}})$, respectively.

Proof: See Appendix VI. \blacksquare

Corollary 2 implies that increasing the number of BS antennas can greatly improve the achievable rate. In particular, both the BS-user link and BS-IRS-user link SNRs grow linearly with N . To get more insights, we derive an upper bound for the achievable rate.

Proposition 5: An upper bound for the achievable rate is given by

$$R_{\text{upper}} = \log_2 \left(1 + \frac{P_{\text{BS}} N (\beta_{\text{B2I2U}} M^2 + 2\sqrt{\beta_{\text{B2I2U}}\beta_{\text{B2U}}} M + \beta_{\text{B2U}} + \sigma_{\text{NLOS}}^2)}{\sigma_0^2} \right). \quad (76)$$

Proof: Starting from Corollary 2 and using the fact that $\sum_{m=1}^M a_m \leq \sum_{m=1}^M |a_m|$, we have

$$\Omega \leq N\beta_{\text{B2I2U}} \sum_{m=1}^M \sum_{n=1}^M |[\mathbf{B}]_{mn}| + 2\sqrt{\beta_{\text{B2I2U}}\beta_{\text{B2U}}} \sum_{m=1}^M \sum_{i=1}^N |[\mathbf{C}]_{mi}| + N\beta_{\text{B2U}} + N\sigma_{\text{NLOS}}^2. \quad (77)$$

Noticing that $|[\mathbf{B}]_{mn}| \leq 1$ and $|[\mathbf{C}]_{mi}| \leq 1$, (76) can be proved. \blacksquare

Proposition 5 indicates that with fixed transmit power, the achievable rate is mainly determined by the numbers of reflecting elements and BS antennas. Specifically, the effective SNR is proportional to the number of BS antennas. Moreover, there is a gain M^2 corresponding to the BS-IRS-user link. This is reasonable because the IRS not only achieves the phase shift beamforming gain of order M in the IRS-user link, but also captures an inherent aperture gain of order M by collecting more signal power in the BS-IRS link. It is worth noting that this M^2 gain only holds when $\sqrt{MA_p} \ll d_{\text{B2I}}$ with A_p being the effective aperture/area of each reflecting element, due to the law of energy conservation [41].

Remark 6: This paper mainly focuses on a single user scenario. However, the proposed angle domain design framework can be easily extended to the multi-user case. For instance, with orthogonal pilot sequences, the proposed angle-domain estimation method can be directly applied to separately estimate the effective angles of each user. Also, the alternating optimization method can be similarly applied to reduce the complexity of beamforming algorithms. The key difference is that, in a multi-user scenario, the co-channel interference should be taken into account. In addition, since all users share the same BS and IRS beamforming vectors, the resultant optimization problem becomes much more complicated.

VI. NUMERICAL RESULTS

In this section, we provide numerical results to illustrate the performance of the angle-domain IRS-aided system, as well as to verify the performance of the proposed ML estimator and the joint optimization scheme. The considered system operates at 2.45 GHz. The large-scale fading coefficient is modeled as $\alpha = L_d^{-\chi}$, where χ is the path loss exponent, and L_d is the transmission distance. We assume the BS is located at the origin. The locations of the user and the IRS are denoted by $(d_{\text{B2U}}, \theta_{\text{B2U}}, \phi_{\text{B2U}})$ and $(d_{\text{B2I}}, \theta_{\text{B2I}}, \phi_{\text{B2I}})$, respectively. For all simulations, unless otherwise specified, the following setup is used: $N = 16$, $M = 256$, $P_{\text{BS}} = 10$ dBm, $\sigma_0^2 = -60$ dBm, $v_{\text{B2U}} = v_{\text{I2U}} = v_{\text{B2I}} = 5$, $\chi_{\text{B2U}} = \chi_{\text{I2U}} = \chi_{\text{B2I}} = 2.5$, IRS location $(42\text{m}, 63^\circ, -16^\circ)$

and user location $(41\text{m}, 47^\circ, -16^\circ)$.

Fig. 2 illustrates the performance of the proposed ML estimator given by Theorem 1, where the analytical results are generated by (24) in Corollary 1. For comparison, the conventional angle-domain estimation method, i.e., the MUSIC method [42], is presented as the benchmark. Note that $\text{MSE}_{x\text{-B2U}}$ and $\text{MSE}_{y\text{-B2U}}$ are defined by $\mathbb{E}\{(\hat{\theta}_{x\text{-B2U}} - \bar{\theta}_{x\text{-B2U}})^2\}$ and $\mathbb{E}\{(\hat{\theta}_{y\text{-B2U}} - \bar{\theta}_{y\text{-B2U}})^2\}$, respectively. As can be readily observed, the numerical results match exactly with the analytical results, thereby validating the correctness of the analytical expressions. Although the MUSIC method is slightly better than the proposed method, it requires more training time and has higher computational complexity than the proposed method. Moreover, as expected in Corollary 1, increasing the number of BS antennas can greatly reduce the mean square error (MSE). This is because with a large number of BS antennas, more angle-related data can be obtained, based on which we can estimate the angles more accurately. In addition, we can see that the MSE is a decreasing function with respect to the Rician K-factor, because a larger Rician K-factor means less uncertainty arising from NLOS paths. Also, as the received SNR becomes larger, the MSE gradually decreases due to less uncertainty caused by noise.

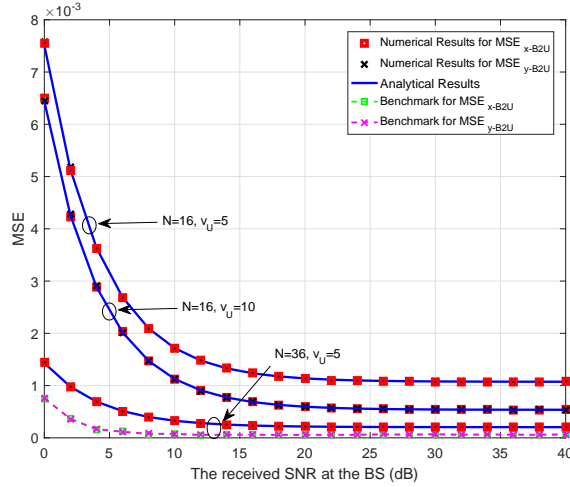


Fig. 2: Performance of the proposed ML estimator.

Fig. 3 illustrates the MSE for the calculated effective angles from the IRS to the user given by Lemma 1, where the analytical results are generated by Theorem 2. Note that $\text{MSE}_{x\text{-I2U}}$ and $\text{MSE}_{y\text{-I2U}}$ are defined by $\mathbb{E}\{(\hat{\theta}_{x\text{-I2U}} - \bar{\theta}_{x\text{-I2U}})^2\}$ and $\mathbb{E}\{(\hat{\theta}_{y\text{-I2U}} - \bar{\theta}_{y\text{-I2U}})^2\}$, respectively. We can see that the numerical curves match the analytical curves well. Besides, the MSE decreases with the received SNR at the BS. This is intuitive because the calculation of effective angles from IRS to

the user relies on the estimated angles from the BS to the user. Moreover, increasing the ratio Ra would severely degrade the accuracy of estimated effective angles. The reason is that a larger Ra means that the user is closer to the IRS, making the calculated angles more sensitive to the estimation error of angles from the BS to the user .

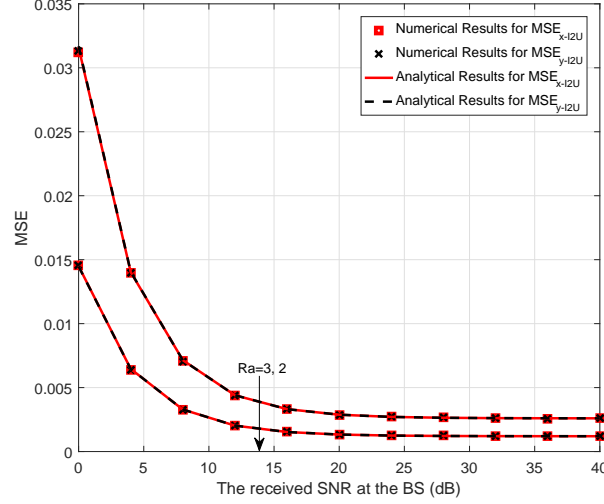


Fig. 3: The MSE for the calculated effective angles from the IRS to the user with IRS location $(57.8\text{m}, 63^\circ, -16^\circ)$.

Fig. 4 illustrates the convergence of the proposed joint beamforming method given by Algorithm 2. As expected in Proposition 4, the proposed algorithm can gradually increase the average received SNR. Moreover, the algorithm converges after only several iterations, making it a low-complexity method. Besides, the received SNR increases as the number of reflecting elements becomes larger, which indicates the benefit of applying a large number of reflecting elements.

Fig. 5 shows the performance of the proposed angle-based beamforming algorithm. For comparison, the algorithm in [15] which assumes full CSI is presented as “Benchmark 1”, while a beamforming algorithm based on angles estimated by the MUSIC method is presented as “Benchmark 2”. As can be seen, our proposed angle-based algorithm achieves nearly the same performance as both benchmark algorithms. The beamforming algorithm corresponding to “Benchmark 1 ” achieves the best performance, but requires full CSI. Although the angle-based beamforming algorithm corresponding to “Benchmark 2 ” is slightly better than the proposed algorithm, it adopts the MUSIC method to estimate angle information and thus has higher training overhead and computational complexity than the proposed angle-domain estimation method.

Fig. 6 depicts the impact of the number of reflecting elements on the beam pattern of the

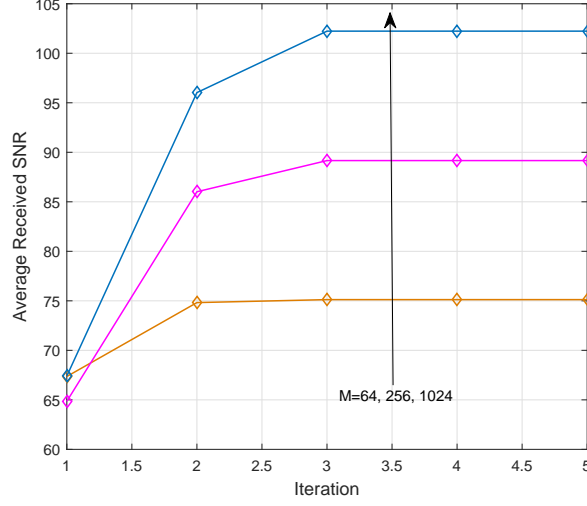


Fig. 4: The convergence of the proposed joint optimization algorithm.

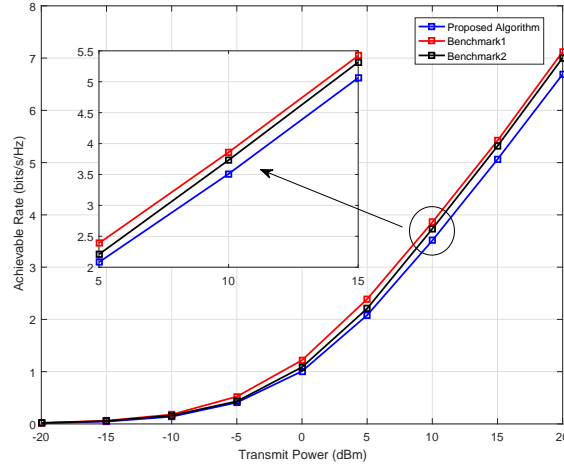


Fig. 5: Performance of the proposed beamforming scheme with $N = 4$ and $M = 36$.

optimized BS beam. As can be observed, with 400 reflecting elements, the main lobe is in the user direction. As the number of reflecting elements increases, the lobe in the user direction gradually becomes smaller and the main lobe appears in the IRS direction, because increasing the number of reflecting elements can enhance the BS-IRS-user link.

Fig. 7 shows the achievable rate of the considered system with different configurations, where the curves associated with “Approximate rate” and “Limit” are plotted according to Corollary 2 and Proposition 5, respectively. As can be readily observed, the three curves corresponding to “Limit”, “Approximate rate” and “With IRS and direct link” have the similar trend, which verifies the effectiveness of our analysis in Corollary 2 and Proposition 5. Moreover, we can see that the achievable rate with IRS is much larger than that without IRS, which indicates the great benefit

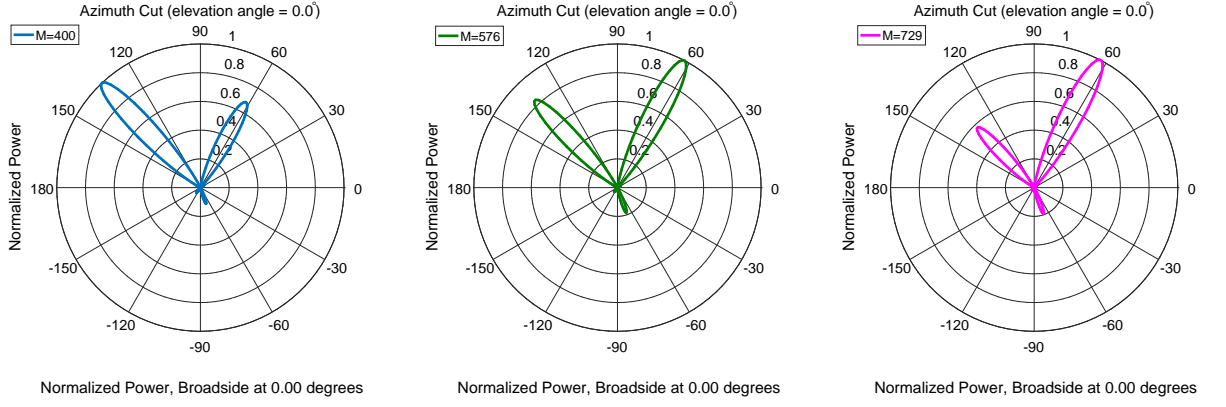


Fig. 6: The impact of the number of reflecting elements on the transmit beam pattern with $N = 36$, user location $(41\text{m}, 133^\circ, -16^\circ)$ and IRS location $(42\text{m}, 63^\circ, -16^\circ)$.

of IRS. Besides, when there is no direct link, the achievable rate becomes extremely low. This is because the acquisition of angle information corresponding to both the BS-IRS and IRS-user links relies on the BS-user direct link. Without the direct link, the BS is not able to obtain any channel information.

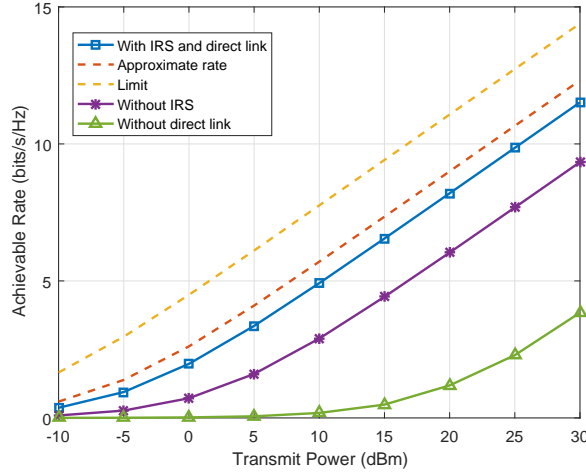


Fig. 7: Achievable rate performance with $N = 4$, $\chi_{B2I} = \chi_{I2U} = 2.3$ and $\chi_{B2U} = 2.8$.

VII. CONCLUSION

This paper considers an IRS-aided system from an angle-domain aspect. The ML estimators for the effective angles from the BS to the user are provided, based on which the effective angles from the IRS to the user are calculated. It has been shown that increasing the number of BS antennas can significantly reduce the estimation error. Also, placing the IRS closer to the BS would lead to a smaller estimation error of the estimated angles from the IRS to the user. Then, exploiting the

estimated angles, a joint optimization algorithm of BS beamforming and IRS beamforming has been proposed, which achieves similar performance to two benchmark algorithms based on full CSI and the MUSIC method respectively. Beam patterns of the optimized BS beam indicate that as the number of reflecting elements becomes larger, the beam becomes more focused towards the IRS direction, as should be expected. Analysis of the achievable rate quantifies the benefit of deploying a large number of BS antennas or reflecting elements. In particular, the BS-user link and the BS-IRS-user link can obtain power gains of order N and NM^2 , respectively.

APPENDIX I

PROOF OF PROPOSITION 1

The received signal at the n -th antenna can be decomposed into the LOS component and the uncertainty component, i.e.,

$$r_n = A_{\text{ob},n} e^{j\vartheta_n} = A_{\text{LOS},n} e^{j(\theta_q + i_{N,n} \bar{\theta}_{x\text{-B2I}} + j_{N,n} \bar{\theta}_{y\text{-B2I}})} + A_{\text{unct},n} e^{j\vartheta_{\text{unct},n}}, \quad (78)$$

where

$$A_{\text{LOS},n} e^{j(\theta_q + i_{N,n} \bar{\theta}_{x\text{-B2I}} + j_{N,n} \bar{\theta}_{y\text{-B2I}})} \triangleq \sqrt{\frac{\alpha_U v_{\text{B2U}}}{v_{\text{B2U}} + 1}} e^{(i_{N,n} \bar{\theta}_{x\text{-B2I}} + j_{N,n} \bar{\theta}_{y\text{-B2I}})q}, \quad (79)$$

$$A_{\text{unct},n} e^{j\vartheta_{\text{unct},n}} \triangleq \sqrt{\frac{\alpha_U}{v_{\text{B2U}} + 1}} \tilde{h}_{\text{B2U},n} q + n_{\text{BS},n}, \quad (80)$$

with $A_{\text{ob},n}$, $A_{\text{LOS},n}$ and $A_{\text{unct},n}$ denoting the corresponding amplitudes and $\vartheta_{\text{unct},n}$ denoting the angle of the uncertainty component.

Furthermore, denote r_n , its LOS component and uncertainty component in a vector form by \vec{a} , \vec{b} and \vec{c} respectively. As such, we have $\vec{a} = \vec{b} + \vec{c}$, yielding a triangle. According to the property of triangles and noticing that e_n is approximately the angle between \vec{a} and \vec{b} , we have $\sin e_n = \frac{A_{\text{unct},n}}{A_{\text{ob},n}} \sin \theta_{\text{ob},n}$, where $\theta_{\text{ob},n} \triangleq \theta_{q,n} + i_{N,n} \bar{\theta}_{x\text{-B2I}} + j_{N,n} \bar{\theta}_{y\text{-B2I}} - \vartheta_{\text{unct},n}$.

Using Taylor expansion, we obtain $e_n = \frac{A_{\text{unct},n}}{A_{\text{ob},n}} \sin \theta_{\text{ob},n}$, where we follow the fact $\lim_{x \rightarrow 0} \sin x = x$.

Due to a large Rician K-factor and a high received SNR at the BS, $A_{\text{unct},n}$ is much smaller than $A_{\text{LOS},n}$. Hence, we have

$$e_n \approx \frac{A_{\text{unct},n}}{A_{\text{LOS},n}} \sin \theta_{\text{ob},n} = \frac{A_{\text{unct},n}}{\sqrt{\frac{\alpha_{\text{B2U}} v_{\text{B2U}} P_q}{v_{\text{B2U}} + 1}}} \sin \theta_{\text{ob},n}. \quad (81)$$

Since $A_{\text{unct},n}$ and $\vartheta_{\text{unct},n}$ are the amplitude and the angle of a complex Gaussian random variable respectively, $A_{\text{unct},n}$ follows Rayleigh distribution and $\theta_{\text{ob},n}$ is uniformly distributed. Therefore, e_n is circularly symmetric Gaussian with the variance given by

$$\sigma_e^2 = \frac{1}{A_{\text{LOS},n}^2} \mathbb{E} \{ |A_{\text{unct},n}|^2 \} \mathbb{E} \{ |\sin \theta_{\text{ob},n}|^2 \} \stackrel{(a)}{=} \frac{(4-\pi)(v_{\text{B2U}}+1)}{8\alpha_{\text{B2U}}P_q v_{\text{B2U}}} \left(\frac{\alpha_{\text{B2U}}P_q}{v_{\text{B2U}}+1} + \sigma_{\text{BS},0}^2 \right), \quad (82)$$

where (a) is derived according to $\mathbb{E} \{ |A_{\text{unct},n}|^2 \} = \frac{4-\pi}{4} \left(\frac{\alpha_{\text{B2U}}P_q}{v_{\text{B2U}}+1} + \sigma_{\text{BS},0}^2 \right)$ and $\mathbb{E} \{ |\sin \theta_{\text{ob},n}|^2 \} = \frac{1}{2}$.

After some algebraic manipulations, we can obtained the desired result.

APPENDIX II

PROOF OF THEOREM 1

Define $\Delta\boldsymbol{\vartheta} \triangleq \left[\Delta\bar{\theta}_{1,m_1}, \dots, \Delta\bar{\theta}_{n,m_n}, \dots, \Delta\bar{\theta}_{\frac{N}{2},m_{\frac{N}{2}}} \right]^T$, and $\bar{\boldsymbol{\theta}} \triangleq [\bar{\theta}_{\text{x-B2U}}, \bar{\theta}_{\text{y-B2U}}]^T$. The conditional probability density function (PDF) of $\Delta\boldsymbol{\vartheta}$ is given by

$$p(\Delta\boldsymbol{\vartheta}; \bar{\boldsymbol{\theta}}) = \prod_{n=1}^{\frac{N}{2}} \frac{1}{\sqrt{2\pi\sigma_{\text{pd}}^2}} \exp \left(-\frac{1}{2\sigma_{\text{pd}}^2} (\Delta\bar{\theta}_{n,m_n} + (i_{N,n} - i_{N,m_n}) \bar{\theta}_{\text{x-B2U}} + (j_{N,n} - j_{N,m_n}) \bar{\theta}_{\text{y-B2U}})^2 \right). \quad (83)$$

According to the Neyman-Fisher Factorization theorem, we factor the above PDF as

$$p(\Delta\boldsymbol{\vartheta}; \bar{\boldsymbol{\theta}}) = f_1(\Delta\boldsymbol{\vartheta}) f_2(\mathbf{T}(\Delta\boldsymbol{\vartheta}), \bar{\boldsymbol{\theta}}), \quad (84)$$

where

$$f_1(\Delta\boldsymbol{\vartheta}) = \frac{1}{(\sqrt{2\pi\sigma_{\text{pd}}^2})^{\frac{N}{2}}} \exp \left(-\frac{1}{2\sigma_{\text{pd}}^2} \sum_{n=1}^{\frac{N}{2}} \Delta\bar{\theta}_{n,m_n}^2 \right), \quad (85)$$

$$f_2(\mathbf{T}(\Delta\boldsymbol{\vartheta}), \bar{\boldsymbol{\theta}}) = \exp \left(-\frac{1}{2\sigma_{\text{pd}}^2} \sum_{n=1}^{\frac{N}{2}} ((i_{N,n} - i_{N,m_n}) \bar{\theta}_{\text{x-B2U}} + (j_{N,n} - j_{N,m_n}) \bar{\theta}_{\text{y-B2U}})^2 \right) \quad (86)$$

$$\times \exp \left(-\frac{1}{\sigma_{\text{pd}}^2} (\bar{\theta}_{\text{x-B2U}} T_1 + \bar{\theta}_{\text{y-B2U}} T_2) \right),$$

$$\mathbf{T}(\Delta\boldsymbol{\vartheta}) = [T_1, T_2]^T. \quad (87)$$

where $T_1 = \sum_{n=1}^{\frac{N}{2}} (i_{N,n} - i_{N,m_n}) \Delta\bar{\theta}_{n,m_n}$ and $T_2 = \sum_{n=1}^{\frac{N}{2}} (j_{N,n} - j_{N,m_n}) \Delta\bar{\theta}_{n,m_n}$.

As such, we obtain a sufficient statistic $\mathbf{T}(\Delta\boldsymbol{\vartheta})$ for $\bar{\boldsymbol{\theta}}$. Thus, $\hat{\bar{\boldsymbol{\theta}}}$ should be a function with respect to $\mathbf{T}(\Delta\boldsymbol{\vartheta})$. Also, noticing that $\hat{\bar{\boldsymbol{\theta}}}$ is unbiased, we obtain $\hat{\bar{\theta}}_{\text{x-B2U}} = -\frac{T_1}{Q_1}$ and $\hat{\bar{\theta}}_{\text{y-B2U}} = -\frac{T_2}{Q_1}$, where

$$Q_1 \triangleq \sum_{n=1}^{N/2} (i_{N,n} - i_{N,m_n})^2 = \frac{1}{6}N(N-1).$$

APPENDIX III

PROOF OF THEOREM 2

We first focus on the derivation of (32). According to Lemma 1, we can express the effective angle from the IRS to the user along x axis as

$$\bar{\theta}_{x-12U} = \frac{\hat{d}_{12U}}{d_{12U}} \hat{\theta}_{x-12U} + \frac{d_{B2U}}{d_{12U}} \epsilon_{x-B2U}, \quad (88)$$

where

$$d_{12U} = \sqrt{\left(x_I - \hat{x}_U - \frac{d_{B2U}}{\pi} \epsilon_{x-B2U}\right)^2 + \left(y_I - \hat{y}_U - \frac{d_{B2U}}{\pi} \epsilon_{y-B2U}\right)^2 + (z_I - z_U)^2}. \quad (89)$$

Recall $z_U = -\frac{d_{B2U} \sqrt{\pi^2 - \bar{\theta}_{x-B2U}^2 - \bar{\theta}_{y-B2U}^2}}{\pi}$. Using the Taylor expansion of $(1+x)^{\frac{1}{2}}$ at $x=0$, we have

$$z_U \approx d_{B2U} \left(-1 + \frac{\bar{\theta}_{x-B2U}^2 + \bar{\theta}_{y-B2U}^2}{2\pi^2}\right) = \hat{z}_U + \frac{d_{B2U} (\epsilon_{x-B2U}^2 + \epsilon_{y-B2U}^2 + 2\epsilon_{x-B2U} \bar{\theta}_{x-B2U} + 2\epsilon_{y-B2U} \bar{\theta}_{y-B2U})}{2\pi^2}. \quad (90)$$

Then, we write $\frac{\hat{d}_{12U}}{d_{12U}}$ as

$$\frac{\hat{d}_{12U}}{d_{12U}} = 1/\sqrt{1+Q_2}, \quad (91)$$

with

$$Q_2 \approx 2 \frac{\frac{d_{B2U}}{\pi} (x_I - \hat{x}_U) \epsilon_{x-B2U} + \frac{d_{B2U}}{\pi} (y_I - \hat{y}_U) \epsilon_{y-B2U} - \frac{d_{B2U}}{\pi^2} (z_I - \hat{z}_U) \left(\hat{\theta}_{x-12U} \epsilon_{x-B2U} + \hat{\theta}_{y-12U} \epsilon_{y-B2U}\right)}{\hat{d}_{12U}^2}.$$

Recall that $\hat{\theta}_{x-12U} = \frac{(x_I - \hat{x}_U)\pi}{\hat{d}_{12U}}$ and $\hat{\theta}_{y-12U} = \frac{(y_I - \hat{y}_U)\pi}{\hat{d}_{12U}}$. We can rewrite Q_2 as

$$Q_2 = \frac{2d_{B2U}}{\pi^2 \hat{d}_{12U}} \left\{ \left(\hat{\theta}_{x-12U} - \frac{\hat{\theta}_{x-12U} \hat{\theta}_{z-12U}}{\pi} \right) \epsilon_{x-B2U} + \left(\hat{\theta}_{y-12U} - \frac{\hat{\theta}_{y-12U} \hat{\theta}_{z-12U}}{\pi} \right) \epsilon_{y-B2U} \right\}, \quad (92)$$

where $\hat{\theta}_{z-12U} \triangleq \frac{(z_I - \hat{z}_U)\pi}{\hat{d}_{12U}}$.

Using the Taylor expansion of $(1+Q_2)^{-\frac{1}{2}}$ at $Q_2=0$, (91) can be approximated as

$$\frac{\hat{d}_{12U}}{d_{12U}} = 1 - \frac{1}{2}Q_2 + o(Q_2) \approx 1 - \frac{1}{2}Q_2. \quad (93)$$

Similarly, we can express $\frac{d_{B2U}}{d_{I2U}}$ as

$$\frac{d_{B2U}}{d_{I2U}} = \frac{d_{B2U}}{\hat{d}_{I2U}} \left(1 - \frac{1}{2} Q_2 \right). \quad (94)$$

Substituting (93) and (94) into (88), we have

$$\begin{aligned} \bar{\theta}_{x-I2U} &= \left(1 - \frac{1}{2} Q_2 \right) \hat{\theta}_{x-I2U} + \frac{d_{B2U}}{\hat{d}_{I2U}} \left(1 - \frac{1}{2} Q_2 \right) \epsilon_{x-B2U} \\ &\stackrel{(a)}{\approx} \left(1 - \frac{1}{2} Q_2 \right) \hat{\theta}_{x-I2U} + \frac{d_{B2U}}{\hat{d}_{I2U}} \epsilon_{x-B2U}. \end{aligned} \quad (95)$$

After some algebraic manipulations, we complete the proof of (32). Following the similar process, we can obtain (33).

APPENDIX IV

PROOF OF PROPOSITION 2

The average received power is given by

$$P_r = \mathbb{E} \left\{ |\mathbf{g}^T \mathbf{w}|^2 \right\} = \mathbb{E} \left\{ |\mathbf{g}_{\text{LOS}}^T \mathbf{w}|^2 \right\} + \mathbb{E} \left\{ |\mathbf{g}_{\text{NLOS}}^T \mathbf{w}|^2 \right\}, \quad (96)$$

where the effective channel is defined as $\mathbf{g}^T = \mathbf{h}_{B2U}^T + \mathbf{h}_{I2U}^T \mathbf{\Theta} \mathbf{H}_{B2I}$ and decomposed as $\mathbf{g}_{\text{LOS}}^T + \mathbf{g}_{\text{NLOS}}^T$ with

$$\mathbf{g}_{\text{LOS}}^T = \sqrt{\frac{\alpha_{I2U} \alpha_{B2I} v_{B2I} v_{I2U}}{(v_{B2I} + 1)(v_{I2U} + 1)}} \mathbf{b}^T (\bar{\theta}_{x-I2U}, \bar{\theta}_{y-I2U}) \mathbf{\Theta} \bar{\mathbf{H}}_{B2I} + \sqrt{\frac{\alpha_{B2U} v_{B2U}}{v_{B2U} + 1}} \mathbf{a}^T (\bar{\theta}_{x-B2U}, \bar{\theta}_{y-B2U}), \quad (97)$$

$$\mathbf{g}_{\text{NLOS}}^T = \sqrt{\frac{\alpha_{B2I} \alpha_{I2U}}{v_{B2I} + 1}} \mathbf{h}_{I2U}^T \mathbf{\Theta} \tilde{\mathbf{H}}_{B2I} + \sqrt{\frac{\alpha_{B2I} \alpha_{I2U} v_{B2I}}{(v_{B2I} + 1)(v_{I2U} + 1)}} \tilde{\mathbf{h}}_{I2U}^T \mathbf{\Theta} \bar{\mathbf{H}}_{B2I} + \sqrt{\frac{\alpha_{B2U}}{v_{B2U} + 1}} \tilde{\mathbf{h}}_{B2U}^T, \quad (98)$$

where $\bar{\mathbf{H}}_{B2I} \triangleq \mathbf{b} (\bar{\theta}_{x-B2Ia}, \bar{\theta}_{y-B2Ia}) \mathbf{a}^T (\bar{\theta}_{x-B2I}, \bar{\theta}_{y-B2I})$.

We start with the calculation of the second term:

$$\mathbb{E} \left\{ |\mathbf{g}_{\text{NLOS}}^T \mathbf{w}|^2 \right\} = \text{tr} (\mathbf{w} \mathbf{w}^H \mathbb{E} \{ \mathbf{g}_{\text{NLOS}}^* \mathbf{g}_{\text{NLOS}}^T \}) = \sigma_{\text{NLOS}}^2 \mathbf{w}^H \mathbf{w}, \quad (99)$$

where

$$\sigma_{\text{NLOS}}^2 = M \frac{\alpha_{I2U} \alpha_{B2I}}{v_{B2I} + 1} \left(1 + \frac{v_{B2I}}{v_{I2U} + 1} \right) + \frac{\alpha_{B2U}}{v_{B2U} + 1}. \quad (100)$$

Then, we calculate the first term:

$$\mathbb{E} \left\{ \left| \mathbf{g}_{\text{LOS}}^T \mathbf{w} \right|^2 \right\} = T_1 + T_2 + 2\text{Re}(T_3), \quad (101)$$

where

$$T_1 = \mathbb{E} \left\{ \mathbf{b}^T (\bar{\theta}_{\text{x-I2U}}, \bar{\theta}_{\text{y-I2U}}) \phi_b \phi_b^H \mathbf{b}^* (\bar{\theta}_{\text{x-I2U}}, \bar{\theta}_{\text{y-I2U}}) \right\}, \quad (102)$$

$$T_2 = \mathbb{E} \left\{ \mathbf{a}^T (\bar{\theta}_{\text{x-B2U}}, \bar{\theta}_{\text{y-B2U}}) \phi_a \phi_a^H \mathbf{a}^* (\bar{\theta}_{\text{x-B2U}}, \bar{\theta}_{\text{y-B2U}}) \right\}, \quad (103)$$

$$T_3 = \mathbb{E} \left\{ \mathbf{a}^T (\bar{\theta}_{\text{x-B2U}}, \bar{\theta}_{\text{y-B2U}}) \phi_a \phi_b^H \mathbf{b}^* (\bar{\theta}_{\text{x-I2U}}, \bar{\theta}_{\text{y-I2U}}) \right\}, \quad (104)$$

with

$$\phi_a \triangleq \sqrt{\frac{v_{\text{B2U}} \alpha_{\text{B2U}}}{v_{\text{B2U}} + 1}} \mathbf{w}, \quad \phi_b \triangleq \sqrt{\frac{v_{\text{B2I}} \alpha_{\text{B2I}} \alpha_{\text{I2U}}}{v_{\text{B2I}} + 1}} \mathbf{\Theta} \bar{\mathbf{H}}_{\text{B2I}} \mathbf{w}. \quad (105)$$

1) Calculate T_1

$$T_1 = \text{tr} (\phi_b \phi_b^H \mathbf{B}) = \phi_b^H \mathbf{B} \phi_b, \quad (106)$$

where $\mathbf{B} \triangleq \mathbb{E} \left\{ \mathbf{b}^* (\bar{\theta}_{\text{x-I2U}}, \bar{\theta}_{\text{y-I2U}}) \mathbf{b}^T (\bar{\theta}_{\text{x-I2U}}, \bar{\theta}_{\text{y-I2U}}) \right\}$ with elements given by

$$[\mathbf{B}]_{mn} = \mathbb{E} \left\{ \exp \left(j (i_{M,n} - i_{M,m}) \bar{\theta}_{\text{x-I2U}} + j (j_{M,n} - j_{M,m}) \bar{\theta}_{\text{y-I2U}} \right) \right\}. \quad (107)$$

Substituting (32) and (33) into (107), we have

$$[\mathbf{B}]_{mn} = \left[\hat{\mathbf{B}} \right]_{mn} \mathbb{E} \left\{ \exp \left(j (i_{M,mn} \varphi_1 + j_{M,mn} \varphi_2) \epsilon_{\text{x-B2U}} + j (i_{M,mn} \varphi_2 + j_{M,mn} \varphi_3) \epsilon_{\text{y-B2U}} \right) \right\}, \quad (108)$$

where $\hat{\mathbf{B}} \triangleq \mathbf{b}^* \left(\hat{\theta}_{\text{x-I2U}}, \hat{\theta}_{\text{y-I2U}} \right) \mathbf{b}^T \left(\hat{\theta}_{\text{x-I2U}}, \hat{\theta}_{\text{y-I2U}} \right)$, $i_{M,mn} \triangleq (i_{M,n} - i_{M,m})$, $j_{M,mn} \triangleq (j_{M,n} - j_{M,m})$.

Noticing that $\epsilon_{\text{x-B2U}}$ and $\epsilon_{\text{y-B2U}}$ follow complex Gaussian distribution $\mathcal{CN}(0, \sigma_{\text{est}}^2)$, (108) can be calculated as

$$[\mathbf{B}]_{mn} = \left[\hat{\mathbf{B}} \right]_{mn} \exp \left(-\frac{1}{2} \sigma_{\text{est}}^2 \left\{ (i_{M,mn} \varphi_1 + j_{M,mn} \varphi_2)^2 + (i_{M,mn} \varphi_2 + j_{M,mn} \varphi_3)^2 \right\} \right). \quad (109)$$

2) Calculate T_2

$$T_2 = \text{tr} (\phi_a \phi_a^H \mathbf{A}) = \phi_a^H \mathbf{A} \phi_a, \quad (110)$$

where $\mathbf{A} \triangleq \mathbb{E} \left\{ \mathbf{a}^* \left(\bar{\theta}_{x-B2U}, \bar{\theta}_{y-B2U} \right) \mathbf{a}^T \left(\bar{\theta}_{x-B2U}, \bar{\theta}_{y-B2U} \right) \right\}$ with elements given by

$$[\mathbf{A}]_{mn} = \mathbb{E} \left\{ \exp \left(j i_{N,mn} \bar{\theta}_{x-B2U} + j j_{N,mn} \bar{\theta}_{y-B2U} \right) \right\}. \quad (111)$$

Invoking the results given by Theorem 2, we have

$$[\mathbf{A}]_{mn} = \left[\hat{\mathbf{A}} \right]_{mn} \mathbb{E} \left\{ \exp \left(j i_{N,mn} \epsilon_{x-B2U} + j j_{N,mn} \epsilon_{y-B2U} \right) \right\}, \quad (112)$$

where $\hat{\mathbf{A}} \triangleq \mathbf{a}^* \left(\hat{\theta}_{x-B2U}, \hat{\theta}_{y-B2U} \right) \mathbf{a}^T \left(\hat{\theta}_{x-B2U}, \hat{\theta}_{y-B2U} \right)$.

Due to the fact that ϵ_{x-B2U} and ϵ_{y-B2U} follow complex Gaussian distribution $\mathcal{CN}(0, \sigma_{\text{est}}^2)$, $[\mathbf{A}]_{mn}$ can be computed as

$$[\mathbf{A}]_{mn} = \left[\hat{\mathbf{A}} \right]_{mn} \exp \left(-\frac{1}{2} \sigma_{\text{est}}^2 \{ i_{N,mn}^2 + j_{N,mn}^2 \} \right). \quad (113)$$

3) Calculate T_3

$$T_3 = \mathbb{E} \left\{ \mathbf{a}^T \phi_a \phi_b^H \mathbf{b}^* \right\} = \text{tr} \left(\phi_a \phi_b^H \mathbf{C} \right) = \phi_b^H \mathbf{C} \phi_a, \quad (114)$$

where $\mathbf{C} \triangleq \mathbb{E} \left\{ \mathbf{b}^* \left(\bar{\theta}_{x-I2U}, \bar{\theta}_{y-I2U} \right) \mathbf{a}^T \left(\bar{\theta}_{x-B2U}, \bar{\theta}_{y-B2U} \right) \right\}$ with elements $[\mathbf{C}]_{mn}$ given by

$$[\mathbf{C}]_{mn} = \mathbb{E} \left\{ \exp \left(j \left\{ i_{M,m} \bar{\theta}_{x-I2U} + j_{M,m} \bar{\theta}_{y-I2U} - i_{N,n} \bar{\theta}_{x-B2U} - j_{N,n} \bar{\theta}_{y-B2U} \right\} \right) \right\}. \quad (115)$$

Invoking the results in Theorem 2, we have

$$[\mathbf{C}]_{mn} = \left[\hat{\mathbf{C}} \right]_{mn} \quad (116)$$

$$\times \mathbb{E} \left\{ \exp \left(j \left(i_{M,m} \varphi_1 + j_{M,m} \varphi_2 - i_{N,n} \right) \epsilon_{x-B2U} + j \left(i_{M,m} \varphi_2 + j_{M,m} \varphi_3 - j_{N,n} \right) \epsilon_{y-B2U} \right) \right\},$$

where $\hat{\mathbf{C}} \triangleq \mathbf{b}^* \left(\hat{\theta}_{x-I2U}, \hat{\theta}_{y-I2U} \right) \mathbf{a}^T \left(\hat{\theta}_{x-B2U}, \hat{\theta}_{y-B2U} \right)$.

According to the fact that ϵ_{x-B2U} and ϵ_{y-B2U} follow complex Gaussian distribution $\mathcal{CN}(0, \sigma_{\text{est}}^2)$, we have

$$[\mathbf{C}]_{mn} = \left[\hat{\mathbf{C}} \right]_{mn} \exp \left(-\frac{1}{2} \sigma_{\text{est}}^2 \left\{ (i_{M,m} \varphi_1 + j_{M,m} \varphi_2 - i_{N,n})^2 + (i_{M,m} \varphi_2 + j_{M,m} \varphi_3 - j_{N,n})^2 \right\} \right). \quad (117)$$

Combining 1), 2) and 3), we have

$$\mathbb{E} \left\{ \left| \mathbf{g}_{\text{LOS}}^T \mathbf{w} \right|^2 \right\} = \phi_b^H \mathbf{B} \phi_b + \phi_a^H \mathbf{A} \phi_a + 2 \text{Re} \left(\phi_b^H \mathbf{C} \phi_a \right), \quad (118)$$

Combining (118) and (99) yields the desired result.

APPENDIX V

PROOF OF PROPOSITION 3

The constant-modulus constraint $|\xi_i| = 1, i = 1, \dots, M$ is equivalent to the following two constraints:

$$\text{tr}(\boldsymbol{\xi}) = M, \quad (119)$$

$$\|\boldsymbol{\xi}_\infty\| \leq 1. \quad (120)$$

Since we project $\mathbf{g}_{\text{gd}} = -\nabla_{\boldsymbol{\xi}} G(\boldsymbol{\xi})$ into the tangent plane of $\text{tr}(\boldsymbol{\xi}\boldsymbol{\xi}^H) = M$: $\mathbf{g}_p = \mathbf{g}_{\text{gd}} - \frac{\mathbf{g}_{\text{gd}}^T \boldsymbol{\xi}^* \boldsymbol{\xi}}{\|\boldsymbol{\xi}\|^2}$, and use \mathbf{g}_p as the search direction, the first constraint $\text{tr}(\boldsymbol{\xi}) = M$ holds. Noticing that $\lim_{p \rightarrow \infty} \ell_p = \ell_\infty$, the constraint $\|\boldsymbol{\xi}_\infty\| \leq 1$ is approximately equivalent to $\|\boldsymbol{\xi}_p\| \leq 1$ with a large p . Then a barrier method is exploited to make $\|\boldsymbol{\xi}_p\| \leq 1$ satisfied. To this end, we complete our proof.

APPENDIX VI

PROOF OF COROLLARY 2

Recall that the optimal \mathbf{w} is $\sqrt{P_{\text{BS}}}\mathbf{t}_{\text{max}}$ with \mathbf{t}_{max} being the eigenvector of \mathbf{T} corresponding to the largest eigenvalue λ_{max} . Thus, the average received signal power is given by $P_r = P_{\text{BS}}\lambda_{\text{max}}$.

Due to the fact that the trace of a matrix is the sum of all eigenvalues, the following equation holds $\text{tr}(\mathbf{T}) = \sum_{n=1}^N \lambda_{T,n}$. Since the channel is sparse, the largest eigenvalue λ_{max} dominates the trace $\text{tr}(\mathbf{T})$. As such, we have $\lambda_{\text{max}} \approx \text{tr}(\mathbf{T})$.

Thus, the achievable rate can be approximated as

$$R_{\text{approx}} = \log_2 \left(1 + \frac{P_{\text{BS}}\text{tr}(\mathbf{T})}{\sigma_0^2} \right). \quad (121)$$

Starting from Theorem 3, $\text{tr}(\mathbf{T})$ can be expressed as

$$\begin{aligned} \text{tr}(\mathbf{T}) = & \beta_{\text{B2I2U}} \sum_{m=1}^M \sum_{n=1}^M \xi_m^* \xi_n [\mathbf{B}]_{mn} \left(\sum_{i=1}^N [\bar{\mathbf{H}}_{\text{B2I}}^*]_{mi} [\bar{\mathbf{H}}_{\text{B2I}}]_{ni} \right) \\ & + 2\sqrt{\beta_{\text{B2I2U}}\beta_{\text{B2U}}} \text{Re} \left\{ \sum_{m=1}^M \xi_m^* \left(\sum_{i=1}^N [\mathbf{C}]_{mi} [\bar{\mathbf{H}}_{\text{B2I}}^*]_{mi} \right) \right\} + N\beta_{\text{B2U}} + N\sigma_{\text{NLOS}}^2. \end{aligned} \quad (122)$$

Recall that $\bar{\mathbf{H}}_{\text{B2I}} = \mathbf{b}(\bar{\theta}_{\text{x-B2Ia}}, \bar{\theta}_{\text{y-B2Ia}}) \mathbf{a}^T(\bar{\theta}_{\text{x-B2I}}, \bar{\theta}_{\text{y-B2I}})$. We can obtain the desired result.

REFERENCES

- [1] C. V. N. Index, "Global mobile data traffic forecast update, 2017–2022 white paper," *Cisco: San Jose, CA, USA*, 2019.
- [2] C. Huang, A. Zappone, G. C. Alexandropoulos, M. Debbah, and C. Yuen, "Reconfigurable intelligent surfaces for energy efficiency in wireless communication," *IEEE Transactions on Wireless Communications*, vol. 18, no. 8, pp. 4157–4170, 2019.
- [3] X. Hu, C. Zhong, Y. Zhu, X. Chen, and Z. Zhang, "Programmable metasurface based multicast systems: Design and analysis," *IEEE Journal on Selected Areas in Communications*, vol. 38, no. 8, pp. 1763–1776, 2020.
- [4] X. Hu, C. Zhong, Y. Zhang, X. Chen, and Z. Zhang, "Location information aided multiple intelligent reflecting surface systems," *IEEE Transactions on Communications*, vol. 68, no. 12, pp. 7948–7962, 2020.
- [5] X. Hu, J. Wang, and C. Zhong, "Statistical csi based design for intelligent reflecting surface assisted miso systems," *Science China: Information Science*, vol. 63, no. 12, p. 222303, 2020.
- [6] J. Zhang, Y. Zhang, C. Zhong, and Z. Zhang, "Robust design for intelligent reflecting surfaces assisted miso systems," *IEEE Communications Letters*, vol. 24, no. 10, pp. 2353–2357, 2020.
- [7] Q. Wu and R. Zhang, "Weighted sum power maximization for intelligent reflecting surface aided SWIPT," *IEEE Wireless Communications Letters*, vol. 9, no. 5, pp. 586–590, 2020.
- [8] E. Björnson, Ö. Özdogan, and E. G. Larsson, "Intelligent reflecting surface vs. decode-and-forward: How large surfaces are needed to beat relaying?" *arXiv preprint arXiv:1906.03949*, 2019.
- [9] Y. Han, W. Tang, S. Jin, C.-K. Wen, and X. Ma, "Large intelligent surface-assisted wireless communication exploiting statistical CSI," *IEEE Transactions on Vehicular Technology*, vol. 68, no. 8, pp. 8238–8242, 2019.
- [10] Q. Wu and R. Zhang, "Towards smart and reconfigurable environment: Intelligent reflecting surface aided wireless network," *IEEE Communications Magazine*, vol. 58, no. 1, pp. 106–112, 2020.
- [11] T. J. Cui, M. Q. Qi, X. Wan, J. Zhao, and Q. Cheng, "Coding metamaterials, digital metamaterials and programmable metamaterials," *Light: Science & Applications*, vol. 3, no. 10, p. e218, 2014.
- [12] C. Liaskos, S. Nie, A. Tsioliaridou, A. Pitsillides, S. Ioannidis, and I. Akyildiz, "A new wireless communication paradigm through software-controlled metasurfaces," *IEEE Communications Magazine*, vol. 56, no. 9, pp. 162–169, 2018.
- [13] J. Chen, Y.-C. Liang, Y. Pei, and H. Guo, "Intelligent reflecting surface: A programmable wireless environment for physical layer security," *IEEE Access*, vol. 7, pp. 82 599–82 612, 2019.
- [14] C. Huang, G. C. Alexandropoulos, A. Zappone, M. Debbah, and C. Yuen, "Energy efficient multi-user MISO communication using low resolution large intelligent surfaces," in *2018 IEEE Globecom Workshops (GC Wkshps)*. IEEE, 2018, pp. 1–6.
- [15] Q. Wu and R. Zhang, "Intelligent reflecting surface enhanced wireless network via joint active and passive beamforming," *IEEE Transactions on Wireless Communications*, vol. 18, no. 11, pp. 5394–5409, 2019.
- [16] —, "Intelligent reflecting surface enhanced wireless network: Joint active and passive beamforming design," in *2018 IEEE Global Communications Conference (GLOBECOM)*. IEEE, 2018, pp. 1–6.
- [17] J. Ye, S. Guo, and M.-S. Alouini, "Joint reflecting and precoding designs for SER minimization in reconfigurable intelligent surfaces assisted MIMO systems," *IEEE Transactions on Wireless Communications*, vol. 19, no. 8, pp. 5561–5574, 2020.
- [18] H. Guo, Y.-C. Liang, J. Chen, and E. G. Larsson, "Weighted sum-rate optimization for intelligent reflecting surface enhanced wireless networks," in *2019 IEEE Global Communications Conference (GLOBECOM)*. IEEE, 2019, pp. 1–6.
- [19] G. Yang, X. Xu, and Y.-C. Liang, "Intelligent reflecting surface assisted non-orthogonal multiple access," in *2020 IEEE Wireless Communications and Networking Conference (WCNC)*. IEEE, 2020, pp. 1–6.
- [20] P. Wang, J. Fang, X. Yuan, Z. Chen, H. Duan, and H. Li, "Intelligent reflecting surface-assisted millimeter wave

- communications: Joint active and passive precoding design,” *IEEE Transactions on Vehicular Technology (Early Access)*, 2020.
- [21] C. Pan, H. Ren, K. Wang, M. ElKashlan, A. Nallanathan, J. Wang, and L. Hanzo, “Intelligent reflecting surface enhanced MIMO broadcasting for simultaneous wireless information and power transfer,” *IEEE Journal on Selected Areas in Communications*, vol. 38, no. 8, pp. 1719–1734, 2020.
- [22] Z. Chu, W. Hao, P. Xiao, and J. Shi, “Intelligent reflecting surface aided multi-antenna secure transmission,” *IEEE Wireless Communications Letters*, vol. 9, no. 1, pp. 108–112, 2020.
- [23] Q. Wu and R. Zhang, “Beamforming optimization for intelligent reflecting surface with discrete phase shifts,” in *ICASSP 2019-2019 IEEE International Conference on Acoustics, Speech and Signal Processing (ICASSP)*. IEEE, 2019, pp. 7830–7833.
- [24] S. Abeywickrama, R. Zhang, and C. Yuen, “Intelligent reflecting surface: Practical phase shift model and beamforming optimization,” *IEEE Transactions on Communications*, vol. 68, no. 9, pp. 5849–5863, 2020.
- [25] X. Yu, D. Xu, D. W. K. Ng, and R. Schober, “IRS-assisted green communication systems: Provable convergence and robust optimization,” *arXiv preprint arXiv:2011.06484*, 2020.
- [26] D. Xu, X. Yu, Y. Sun, D. W. K. Ng, and R. Schober, “Resource allocation for IRS-assisted full-duplex cognitive radio systems,” *arXiv preprint arXiv:2003.07467*, 2020.
- [27] Y. Zhang, C. Zhong, Z. Zhang, and W. Lu, “Sum rate optimization for two way communications with intelligent reflecting surface,” *IEEE Communications Letters*, vol. 25, no. 5, pp. 1090–1094, 2020.
- [28] H. Shen, W. Xu, S. Gong, Z. He, and C. Zhao, “Secrecy rate maximization for intelligent reflecting surface assisted multi-antenna communications,” *IEEE Communications Letters*, vol. 23, no. 9, pp. 1488–1492, 2019.
- [29] Q.-U.-A. Nadeem, A. Kammoun, A. Chaaban, M. Debbah, and M.-S. Alouini, “Intelligent reflecting surface assisted multi-user MISO communication,” *arXiv preprint arXiv:1906.02360*, 2019.
- [30] B. Zheng and R. Zhang, “Intelligent reflecting surface-enhanced OFDM: Channel estimation and reflection optimization,” *IEEE Wireless Communications Letters*, vol. 9, no. 4, pp. 518–522, 2020.
- [31] Z.-Q. He and X. Yuan, “Cascaded channel estimation for large intelligent metasurface assisted massive MIMO,” *IEEE Wireless Communications Letters*, vol. 9, no. 2, pp. 210–214, 2020.
- [32] D. Mishra and H. Johansson, “Channel estimation and low-complexity beamforming design for passive intelligent surface assisted MISO wireless energy transfer,” in *ICASSP 2019-2019 IEEE International Conference on Acoustics, Speech and Signal Processing (ICASSP)*. IEEE, 2019, pp. 4659–4663.
- [33] L. Subrt and P. Pechac, “Intelligent walls as autonomous parts of smart indoor environments,” *IET communications*, vol. 6, no. 8, pp. 1004–1010, 2012.
- [34] T. Abdelrahman, A. Muhammad, and A. Ahmed, “Energy efficient multi-user MISO communication using low resolution large intelligent surfaces,” in *2019 IEEE Global Communications Conference (GLOBECOM)*. IEEE, 2019, pp. 1–6.
- [35] T. Abdelrahman, M. Alrabeiah, and A. Ahmed, “Enabling large intelligent surfaces with compressive sensing and deep learning,” *arXiv preprint arXiv:1904.10136*, 2019.
- [36] D. Xu, X. Yu, V. Jamali, D. W. K. Ng, and R. Schober, “Resource allocation for large IRS-assisted SWIPT systems with non-linear energy harvesting model,” *arXiv preprint arXiv:2010.00846*, 2020.
- [37] M. Jian, F. Gao, Z. Tian, S. Jin, and S. Ma, “Angle-domain aided UL/DL channel estimation for wideband mmwave massive MIMO systems with beam squint,” *IEEE Transactions on Wireless Communications*, vol. 18, no. 7, pp. 3515–3527, 2019.

- [38] W. Shao, S. Zhang, H. Li, N. Zhao, and O. A. Dobre, "Angle-domain NOMA over multicell millimeter wave massive MIMO networks," *IEEE Transactions on Communications*, vol. 68, no. 4, pp. 2277–2292, 2020.
- [39] F. Dong, W. Wang, Z. Huang, and P. Huang, "High-resolution angle-of-arrival and channel estimation for mmwave massive MIMO systems with lens antenna array," *IEEE Transactions on Vehicular Technology*, vol. 69, no. 11, pp. 12 963–12 973, 2020.
- [40] M. Simic and P. Pejovic, "Positioning in cellular networks," in *Cellular Networks—Positioning, Performance Analysis, Reliability*. InTech, 2011, p. 51.
- [41] E. Björnson and L. Sanguinetti, "Demystifying the power scaling law of intelligent reflecting surfaces and metasurfaces," in *2019 IEEE 8th International Workshop on Computational Advances in Multi-Sensor Adaptive Processing (CAMSAP)*. IEEE, 2019, pp. 549–553.
- [42] H. L. V. Trees, *Optimum Array Processing, Part IV of Detection, Estimation, and Modulation Theory*. New York: Wiley, 2002.